Analogue modeling of lithospheric-scale orocline buckling: Constraints on the evolution of the Iberian-Armorican Arc

Daniel Pastor-Galán[1,†], Gabriel Gutiérrez-Alonso[1], Gernold Zulauf[2], and Friedhelm Zanella[3]
[1]*Departamento de Geología, Universidad de Salamanca, Facultad de Ciencias, 37008, Salamanca, Spain*
[2]*Institut für Geowissenschaften, Goethe-Universität, Campus Riedberg, Altenhöferallee 1, 60438, Frankfurt am Main, Germany*
[3]*Institut für Neuroradiologie, Goethe-Universität, Schleusenweg 2-16, Haus 95, 60528, Frankfurt am Main, Germany*

ABSTRACT

We report on a series of analogue modeling experiments that study the oroclinal buckling process as a thick-skinned process involving the entire lithosphere. The results obtained in the experiments suggest that, during oroclinal buckling, extension in the outer arc and significant shortening in the inner arc are produced by tangential longitudinal strain as the main mechanism of deformation. The models also reveal that the mantle lithosphere thickens in different noncylindrical ways depending on the initial lithospheric mantle thickness: from almost recumbent to folding with subvertical axial planes for the thinnest to the thickest mantle lithosphere, respectively. The results provide useful insights into thick-skinned orocline buckling as it is interpreted to have happened in the Iberian-Armorican Arc.

INTRODUCTION

Although the concept of plate tectonics revolutionized the understanding of regional crustal processes, the behavior of the mantle lithosphere during plate-margin interaction is still poorly understood. Most of our recent understanding of the dynamics of the mantle lithosphere during tectonic processes has been obtained from geophysical studies (e.g., Karato and Wu, 1993) and by analogue modeling (e.g., Davy and Cobbold, 1991). In addition, orogenic processes at lithospheric scale have been analyzed by numerical modeling (e.g., Houseman et al., 1981; Schott and Schmeling, 1998; Arnold et al., 2001; Beaumont et al., 2001; Morency et al., 2002; Moresi et al., 2002; Pysklywec et al., 2002, 2006; Morency and Doin, 2004). Although the numerical models yield interesting results and have provided impressive insights into lithospheric mantle dynamics, especially in subduction-related environments, they have not, as yet, produced accurate and robust three-dimensional (3-D) numerical approximations of the complex processes affecting the whole lithosphere.

Analogue modeling, on the other hand, is a powerful technique that can be used to study geological processes in 3-D (e.g., Ghosh et al., 1995; Zulauf et al., 2003, 2011a, 2011b; Zulauf and Zulauf, 2005; Dietl and Koyi, 2011) if the models are properly scaled (Hubbert, 1937; Weijermars and Schmeling, 1986). These models can be used to study tectonic processes from micro- to lithospheric scale (e.g., Autin et al., 2010; Fernández-Lozano et al., 2011).

Orogens extend hundreds to thousands of kilometers across Earth's surface, and although many are approximately linear in plan, most are curved or bent when observed in map view. Many bends are significant deflections, both in terms of scale and magnitude. The western part of the Variscan orogen of Europe, for example, is characterized by a 180° hairpin bend that affects a 500-km-wide mountain system in Iberia and France, as previously recognized in the late nineteenth century by Suess (1885). Recent paleomagnetic data indicate that this mountain system originated as an approximately linear belt (Weil et al., 2000, 2001, 2010), and hence it is an orocline. The origin of this orocline has been the subject of debate for decades. This bend of the Variscan mountain system, formed in the Pennsylvanian, is temporally associated with a pervasive thermal and magmatic event that affected large parts of central Pangea (Gutiérrez-Alonso et al., 2004). Modern bends are equally impressive and are potentially of equivalent geological significance. Some of the greatest topographic reliefs on Earth are associated with the still-evolving tight bends (called syntaxes) that adorn, for example, the eastern and western terminations of the Himalayas (Burg and Podladchikov, 2000) or the Cape fold belt in South Africa (e.g., Johnston, 2000). These syntaxes are characterized by elevated heat flow and are the sites of exhumation of large tracts of lower crust (Zeitler et al., 2001). Likewise, Earth's second largest and highest plateau, the Altiplano of South America, reached its present elevation during formation of the great Bolivian bend of the Andes (Allmendinger et al., 1997; Isacks, 1988; Maffione et al., 2009).

Analogue modeling has been previously performed to understand mechanisms leading to curved orogens in several possible scenarios. One of the most common models invoked to produce curved orogens is the collision of a rigid indentor (microplate) with a continental margin, the latter of which shows a linear structural grain. This scenario has been frequently modeled using simple rock analogues (e.g., Tapponnier et al., 1982; Marshak, 1988; Davy and Cobbold, 1988; Keep, 2000). Other mechanisms propose orogenic curvature to be the result of nonparallel thin-skinned transport at uppermost crustal levels. The approaches used to support such a scenario include: (1) the modeling of the curvature of the Cantabrian zone in NW Iberia (Julivert and Arboleya, 1984, 1986); (2) the tracking of thicknesses of the different layers in a foreland fold-and-thrust belt and their relationships to the initiation of thrusts and the possibility of curved resultant geometries (Marshak and Wilkerson, 1992); and (3) the relationships between curved fold-and-thrust belts and previous topography (Marques et al., 2002). However, to the best of our knowledge, there have been no attempts to model lithospheric-scale true oroclines developed from an initially linear orogenic architecture, with the exception of the classic indentor models (e.g., Tapponnier et al., 1982) used to explain the sinuous trend of the Himalayan belt.

There are different rock analogues that can be used to model deformation at crustal and lithospheric scales. Granular materials, such as sand or glass beads, are effective in modeling the upper crust, where the strength of quartzofeldspathic rocks is largely controlled by confining pressure (e.g., Malavieille, 2010). Viscous

†E-mail: dpastorgalan@usal.es

GSA Bulletin; July/August 2012; v. 124; no. 7/8; p. 1293–1309; doi: 10.1130/B30640.1; 9 figures; 3 tables; Data Repository item 2012190

rock analogues, on the other hand, are used to model deformation at deeper structural levels, where the strength is controlled by temperature and strain rate. Plasticine can be used to model power-law creep of rocks undergoing dislocation creep (Zulauf and Zulauf, 2004).

In the present study, we used plasticine as rock analogue in a thermally controlled modeling apparatus, in order to model the lithospheric-scale effects of buckling around a vertical axis and the generation of lithospheric-scale oroclines. The results obtained are compared with the models recently proposed for the evolution of the Iberian-Armorican Arc (Brun and Burg, 1982; Gutiérrez-Alonso et al., 2004, 2011a, 2011b; Weil et al., 2010).

GEOLOGICAL BACKGROUND

Oroclines were firstly described by Carey (1955, p. 257) as "an orogenic system that has been flexed in plan to a horse-shoe or elbow shape." In its first definition, Carey used the word orocline in reference to originally linear orogens that had been bent during a subsequent deformation event. The term orocline was, however, commonly used in the literature as a geometric term for any orogenic curvature, because of the difficulties in constraining the deformation phases and consequently in determining if the orogen had originally been linear (Eldredge et al., 1985). Weil and Sussman (2004) proposed a classification for curved orogens based on kinematics, in contrast to other traditional classifications, which are largely based on the relationship and geometry of displacement and strain trajectories (e.g., Ries and Shackleton, 1976; Marshak, 1988; Ferrill and Groshong, 1993). This classification proposes three kinematic categories of curved orogens: (1) Primary arcs are initially curved belts that have not undergone subsequent rotation around a vertical axis; (2) progressive arcs are belts that have increased their curvature from an original curved shape during their formation; and (3) oroclines are purely secondary curved orogens, i.e., they acquired a curved shape from an initially linear, or almost linear, structural grain.

Constraining the kinematics of curved orogens is not a simple task. Paleomagnetic studies have long been used for unraveling vertical-axis rotations (e.g., Irving and Opdyke, 1965; Grubbs and Van der Voo, 1976; Eldredge et al., 1985; Butler et al., 1995; Weil et al., 2000, 2010), but as discussed by Gray and Stamatakos (1997), the interpretation of paleomagnetic data in complex curved orogenic belts is not straightforward. This difficulty in interpreting the paleomagnetic data arises from the fact that it is not always possible to know the relative timing of magnetization acquisition (MacDonald, 1980; Stewart, 1995; Weil and Van der Voo, 2002), in which case detailed structural analysis is a helpful alternative tool with which to estimate rotations and to investigate the kinematics of curved orogens. For example, orientation of calcite twins (Kollmeier et al., 2000), strain analysis (Ries and Shackleton, 1976; Yonkee and Weil, 2010), anisotropy of magnetic susceptibility (Weil and Yonkee, 2009), and joint analysis (Engelder and Geiser, 1980; Pastor-Galán et al., 2011) have been used to constrain the kinematic evolution of curved orogens where paleomagnetic data are inconclusive.

Furthermore, the kinematic classification of curved orogens does not consider the mechanisms causing the curvatures. These mechanisms might include: (1) initial configuration of the sedimentary basin (e.g., Allmendinger et al., 1990; Mitra, 1997), (2) changes in strength along detachments horizons (Marshak, 2004), (3) buttress effects (Lash, 1988; Paulsen and Marshak, 1999), (4) indentor tectonics (Treloar and Coward, 1991; Jacobs and Thomas, 2004; Ribeiro et al., 2007), (5) wrench faulting (Lawrence et al., 1981; Cunningham, 1993), (6) lateral variations in lithospheric strength across mountain belts (Willingshofer and Sokoutis, 2009), and (7) buckling mountain belts and ribbon continents (Johnston, 2001; Gutiérrez-Alonso et al., 2004).

The Iberian-Armorican Arc of western Europe (Bard et al., 1968; Ribeiro et al., 1995) is one of the most striking curved orogenic systems on Earth, tracing a bend of 180° in the Variscan structural grain (Weil et al., 2001) (Fig. 1). The Iberian-Armorican Arc is situated within the western European Variscan belt, which resulted from Devonian–Carboniferous collision among Gondwana, Laurentia, and several microplates (e.g., Martínez-Catalán et al., 1997, 2007, 2009; Matte, 2001). The impressive geometry of the Iberian-Armorican Arc was first recognized by Suess (1885) and has been the object of many studies (Brun and Burg, 1982; Dias and Ribeiro,

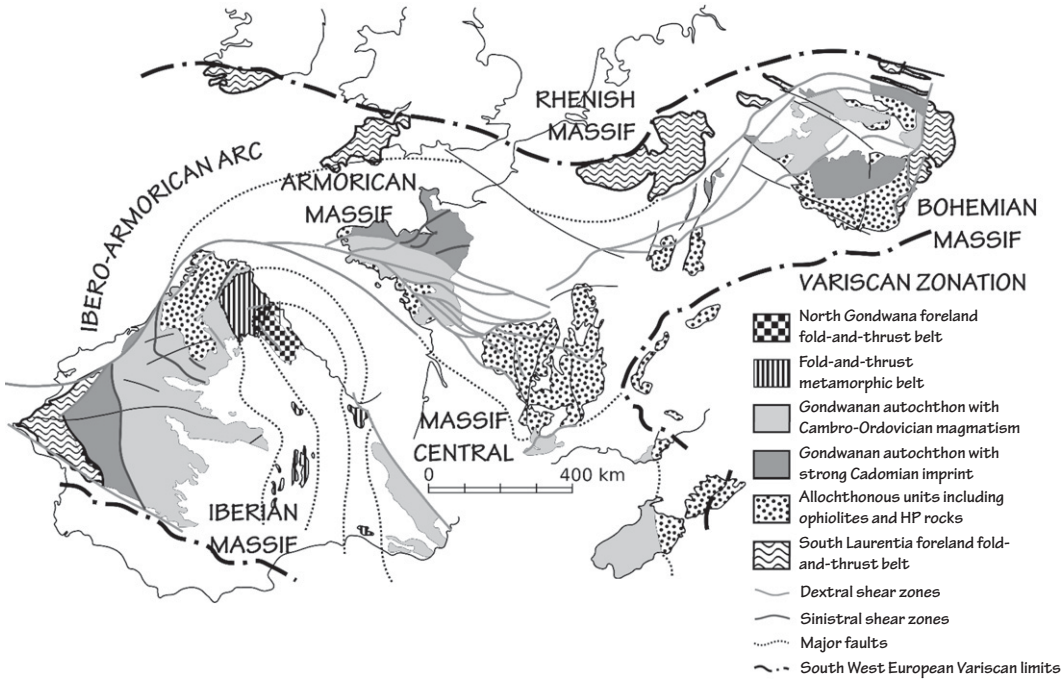

Figure 1. Tectonostratigraphic location of the Iberian-Armorican Arc (after Weil et al., 2010; Pastor-Galán et al., 2011) showing the Iberian-Armorican Arc trace and the main structures related to its formation.

1995), especially at its core (e.g., Julivert, 1971; Julivert and Arboleya, 1984, 1986; Pérez-Estaún et al., 1988; Weil et al., 2000, 2001; Weil, 2006). The aforementioned studies have attempted to decipher the curved mountain belt kinematics, and a wealth of different hypotheses, spanning the entire classification of Weil and Sussman (2004), has been proposed: (1) a primary arc inherited from a Neoproterozoic embayment (Lefort, 1979); (2) a progressive arc resulting from indentation of a point-shaped block situated either in Gondwana (e.g., Matte and Ribeiro, 1975; Brun and Burg, 1982; Dias and Ribeiro, 1995) or in Avalonia (Simancas et al., 2009); (3) an oblique collision producing a noncylindrical orogen (Martínez-Catalán, 1990); (4) a thin-skinned origin produced by a progressive change in the transport direction of the thrust units similar to a photographic iris (Pérez-Estaún et al., 1988); and more recently (5) a true orocline formed by the rotation around a vertical axis of an originally linear orogen (Weil, 2006; Weil et al., 2000, 2010; Gutiérrez-Alonso et al., 2004, 2008). The last hypothesis is the one that we investigate in the present work.

Gutiérrez-Alonso et al. (2004) proposed a thick-skinned kinematic model for the Iberian-Armorican Arc that integrates structural, geochronological, geochemical, magmatic, and paleomagnetic data. This model invokes E-W shortening (in present-day coordinates) (i.e., Pérez-Estaún et al., 1991) that produced the initially linear or almost linear Variscan orogen. Subsequent N-S shortening (e.g., Julivert and Marcos, 1973; Weil et al., 2001, 2010; Merino-Tome et al., 2009) led to lithospheric-scale rotation of the orogen limbs. Buckling was accommodated by local and regional thrust rotation and conical folding of the thrust units around E-W axes that produced interference folds in the inner arc when superposed on longitudinal N-S–trending structures (Julivert and Marcos, 1973; Julivert and Arboleya, 1984; Álvarez-Marron and Pérez-Estaún, 1988) and the development of crustal-scale shear zones in the outer arc (Gutiérrez-Alonso et al., 2010). At a lithospheric scale, the model infers mantle lithosphere thinning below the outer arc and thickening beneath the inner arc based on a tangential longitudinal strain distribution for buckling (Ries and Shackleton, 1976; Gutiérrez-Alonso et al., 2004). Since this thickened lithospheric root is not observed in deep seismic sections (Pérez-Estaún et al., 1994), lithosphere thickening beneath the inner arc might have resulted in a gravitational instability, causing oroclinal development to be followed by mantle lithosphere removal from the lower crust (Gutiérrez-Alonso et al., 2004). Mantle lithosphere removal would have led to upwelling of the asthenosphere, with the associated increase in heat flow. Based on geological (Pastor-Galán et al., 2011) and paleomagnetic constraints (Van der Voo et al., 1997; Weil et al., 2000, 2001, 2010), Iberian-Armorican orocline buckling took place from 310 to 300 Ma in Pennsylvanian time.

This model is based on the kinematic observations and consequences of orocline buckling and does not consider tectono-mechanical aspects of the buckling. Gutiérrez-Alonso et al. (2008) suggested that the self-subduction of the Pangea global plate could have produced the change in the stress field required for orocline buckling. In the latter model, Pangea's oceanic lithosphere subducted northward beneath the portion of Pangea occupied by Siberia. This scenario would have produced extension in the outer parts of Pangea and shortening near the vertex of the northern Paleotethys subduction zone. According to paleogeographic reconstructions of Stampfli and Borel (2002), the Iberian-Armorican Arc was situated in the core of Pangea at the apex of the Paleotethys. Subduction near the apex should have resulted in bending of the lithosphere around a vertical axis. Moreover, the self-subduction model explains (1) dextral faulting in the Iberian-Armorican belt (Gutiérrez-Alonso et al., 2010), (2) Pennsylvanian N-S shortening in the Cantabrian-Asturian arc, (3) large-scale extension in the outer parts of Pangea that resulted in radial rift zones, and (4) the rift-to-drift transition of the Cimmerian ribbon continent.

In addition, evidence for an intense post-orogenic magmatic event (310–290 Ma) has been detected during and after orocline buckling. Evidence for elevated heat flow includes: (1) the widespread post-tectonic granitoids in the Iberian-Armorican Arc and their particular spatial-temporal distribution (Fernández-Suárez et al., 2000, 2011; Gutiérrez-Alonso et al., 2011b); (2) uncommonly high coal ranks in uppermost Carboniferous continental basins (Colmenero and Prado, 1993; Colmenero et al., 2008); (3) gold mineralizations in the foreland fold-and-thrust belt (Martin-Izard et al., 2000); (4) remagnetizations due to unexpected heat flow in the Pennsylvanian and in the Permian (Weil and Van der Voo, 2002); (5) dolomitization along late breaching and out-of-sequence thrusts (Gasparrini et al., 2003); and (6) post-orogenic elevation of the topography (Muñoz-Quijano and Gutiérrez-Alonso, 2007a, 2007b).

Any tectonic model must also consider the rapid rotation of the structures in the uppermost Carboniferous strata and the thermal imprints during Pennsylvanian and early Permian times. Models assuming an initial curvature (Hirt et al., 1992) or models proposing thin-skinned progressive arc development (Pérez-Estaún et al., 1988) are not supported by paleomagnetic data (Weil et al., 2001; Weil, 2006). Indentor-based models require significant thick-skinned block rotation during collision (i.e., in the Devonian). In addition, the foreland, being the place where the deformation took place during the late stages of orogeny (Dallmeyer et al., 1997), would not have exhibited a linear grain, as is suggested by the structural and paleomagnetic data.

Broad knowledge of the geology and the lithospheric response after Iberian-Armorican Arc orocline buckling makes it a natural laboratory in which to study the ways in which the mantle lithosphere could have behaved during thick-skinned orocline buckling. From this point of view, the only way to investigate the lithospheric geometry acquired during lithospheric buckling around a vertical axis is to develop models, either numerical or analogue, that can shed light on this process. The analogue modeling performed in this work illustrates the development of lithospheric roots linked to thick-skinned orocline development.

MODEL SETUP

Analogue Material Properties and Scaling

The orocline development was modeled as a thick-skinned buckling scenario in order to understand the kinematic and dynamic evolution of the lithospheric mantle and the resultant morphologies during and after orocline formation, and to test if these results are consistent with the available paleomagnetic, structural, petrological, and geochronological data and interpretations.

Scaling and construction of the orocline buckling models followed the methodology of Davy and Cobbold (1991) and Cobbold and Jackson (1992) for lithospheric thermomechanical modeling. The experiments were scaled to the natural boundary conditions by selecting proper dimensions and types of analogue materials in order to establish similarity in geometry, kinematics, and dynamics.

The analogue materials selected for the experiments were plasticine and sand. In general terms, plasticine is a nonlinear, strain-rate softening material consisting of a weak organic matrix and mineral fillers (e.g., McClay, 1976; Weijermars, 1986; Schöpfer and Zulauf, 2002; Zulauf and Zulauf, 2004). Plasticine at constant temperature shows non-Newtonian creep defined by the flow law:

$$\dot{E} = C\,\sigma^{n},$$

where $\dot{E}$ is the strain rate, C is a material constant, σ is the stress, and n is the stress exponent

(McClay, 1976). Plasticine is well recognized as a good analogue for rocks undergoing dislocation creep (Zulauf and Zulauf, 2004), which is the dominant deformation mechanism in the lower crust and upper mantle (e.g., Carter and Tsenn, 1987; Hirth et al., 2001; Eaton et al., 2009). Dry sand with rounded grains of quartz and feldspar, on the other hand, was used to model the upper crust. Because of their low cohesion and internal friction angle, according with the Navier-Coulomb and Byerlee law ($\tau = C + \mu\sigma_n$, where τ is the shear stress at failure, C is the cohesive strength of the material, μ is the coefficient of internal friction, and σ_n is the normal stress on the plane at failure), granular materials such as sand are considered suitable analogues for the brittle upper crust (Mandal et al., 1977; McClay and Ellis, 1987; Davy and Cobbold, 1991; Rossi and Storti, 2003). Properties are summarized in Table 1.

Two different kinds of plasticine were used for the experiments (Fig. 2C): (1) Beck's orange, manufactured by Beck's Plastilin, Gomaringen, Germany, and (2) Weible red, made by Weible KG, Schorndorf, Germany. The rheological properties of the selected plasticines (Table 1; Fig. 3) have been studied in previous research and are well constrained (Zulauf and Zulauf, 2004; Tkalcec, 2010), and additional insights are provided by new data from this study. We used an experimental setup that provided temperatures leading to appropriately scaled viscosities for modeling thick-skinned processes. At the temperatures used for the experiments, the stress exponent of the rock analogues is comparable with the stress exponent assumed for lower crust, lithospheric mantle, and asthenosphere, with the exponent value ranging from 2 to 5 (Carter and Tsenn, 1987; Karato and Wu, 1993; Freed et al., 2006).

The asthenosphere was modeled with Beck's orange plasticine, which flows at nearly steady state under experimental strain rates (Zulauf and Zulauf, 2004). Assuming an average viscosity $\eta_{eff} = 5.15 \times 10^{19}$ Pa·s for the asthenosphere (Rydelek and Sacks, 1988; Morency and Doin, 2004), the model is defined with a scale ratio of $M^* = (\eta_{eff})_m/(\eta_{eff})_n = 1.146 \times 10^{-17}$ for Beck's orange at an experimental average temperature $T = 60$ °C based on an effective viscosity of 590 Pa·s for Beck's at 60 °C (Table 1) (where M^* is the viscosity scaling factor and subscripts m and n refer to laboratory model and natural scales, respectively). Density of this plasticine is $\rho = 1250$ kg/m^3, measured at $T = 20$ °C, as plasticine shows minimum decay in density with temperature (Zulauf and Zulauf, 2004). Assuming a density for natural asthenosphere $\rho = 3100$ kg/m^3 (Pysklywec and Cruden, 2004), the resulting density scaling factor is $P^* = \rho_m/\rho_n = 0.4$.

Weible red plasticine was used to model the lithospheric mantle. Assuming an average viscosity $\eta_{eff} = 5 \times 10^{21}$ Pa·s for the natural lithospheric mantle (e.g., Walcott, 1970; Morency and Doin, 2004; Shi and Cao, 2008; Johnson et al., 2007; Fernández-Lozano et al., 2011), the viscosity scaling factor with Weible red at the average temperature ($T = 45$ °C) of the experiments is again $M^* = (\eta_{eff})_m/(\eta_{eff})_n = 1.146 \times 10^{-17}$. Considering the density of this plasticine ($\rho = 1400$ kg/m^3), its scaling ratio with the natural lithospheric mantle ($\rho = 3360$ kg/m^3) is $P^* = \rho_m/\rho_n = 0.41$.

Sand and Beck's orange plasticine were used for upper and lower crust, respectively. Beck's orange was selected to simulate a more ductile and less dense layer than the material used for the lithospheric mantle, and sand was selected to simulate the brittle upper crust. With the same viscosity and density scaling factors, this implies lower-crustal viscosities and densities of ~1.13×10^{21} and 3100 kg/m^3 for model temperatures in the lower crust of 40 °C. These parameters are accepted for a strong lower crust after an orogeny (Carter and Tsenn, 1987; Copley et al., 2011). The rheological and density data for the analogue materials are listed in Table 2.

During the orocline buckling experiments, the temperature varied between 55 °C and 65 °C in the analogue asthenosphere, between 45 °C and 55 °C in the analogue lithospheric mantle, between 40 °C and 45 °C in the lower crust layer, and between 35 °C and 40 °C in the upper crust analogue. The thermal diffusivity of plasticine ranges between 0.65 and 0.8 W m^{-1} K^{-1} (Touloukian et al., 1970). The activation energy has been determined at 323 ± 34 kJ/mol for Beck's orange plasticine and between 400 and 500 kJ/mol for other plasticines (Zulauf and Zulauf, 2004). These values are in agreement with the values proposed for modeling the lithosphere by Davy and Cobbold (1991) and Cobbold and Jackson (1992).

Orocline Buckling Experiment

Fourteen elongated layered models (Ob-1–Ob-14), with varying strain rates, different configurations for the lithospheric mantle, and an approximately constant temperature profile (Fig. 3B) were deformed using a thermomechanical apparatus at the Geozentrum at Frankfurt University (Fig. 2B).

Thermomechanical Deformation Apparatus

The apparatus is capable of simulating tectonic processes at different spatial and temporal scales by applying stresses and adding a thermal gradient to the rock analogues. The apparatus is based on the design of a 3-D coaxial deformation apparatus that works at room temperature (Zulauf

TABLE 1. DENSITY AND RHEOLOGICAL DATA OF THE MATERIALS USED

	Temperature (°C)	Density (kg/m^3)	Effective viscosity (Pa·s)	Stress exponent (n)	Strain rate (s^{-1})	Differential strength (Pa)
Beck's orange						
	20	1250	8.10×10^6*	7.8*	0.001*	
	40		12,900	4.43	0.01	1.29
	45		9610	4.21	0.01	0.961
	50		7330	3.93	0.01	0.733
	55		1700	3.77	0.01	0.17
	60		590	3.41	0.01	0.059
Weible red						
	21	1400				
	40		72,300	4.83	0.01	7.23
	45		57,300	4.37	0.01	5.73
	50		36,500	3.81	0.01	3.65
	55		21,900	3.85	0.01	2.19
	60		16,600	4.61	0.01	1.66
		Bulk density (kg/m^3)	Angle of internal friction	Cohesion (Pa)	Grain size (mm)	
Sand		1200	30.9°	17.8	0.5	21.3

*Data are taken from Zulauf and Zulauf (2004) and were obtained using uniaxial compression, while the other measurements were obtained using a rheometer (RheolabQC).

et al., 2003). Figure 2 depicts a plan view of the machine, which is composed of four aluminum plates set up orthogonally (1, 2, 3, and 4, in Fig. 2A) built on an aluminum table with a copper-plate inlay (5 in Fig. 2A). Two independent motors, connected to the plates by worm gears, achieve the movement of plates 1 and 2 in two orthogonal directions, respectively. One of the motors (motor 1) is fixed to the aluminum table plate (7 in Fig. 2A). Motor 2 is built on a rail and moves passively along the rail when motor 1 is working (8 in Fig. 2A). Plate 3 moves passively when the mobile motor is active, and plate 4 (in Fig. 2A) is attached to the fixed working bench. The speeds of the plates are adjustable and range from 1 to 800 mm/h. The apparatus includes an oven that is capable of heating the basal copper plate from room temperature to 100 °C.

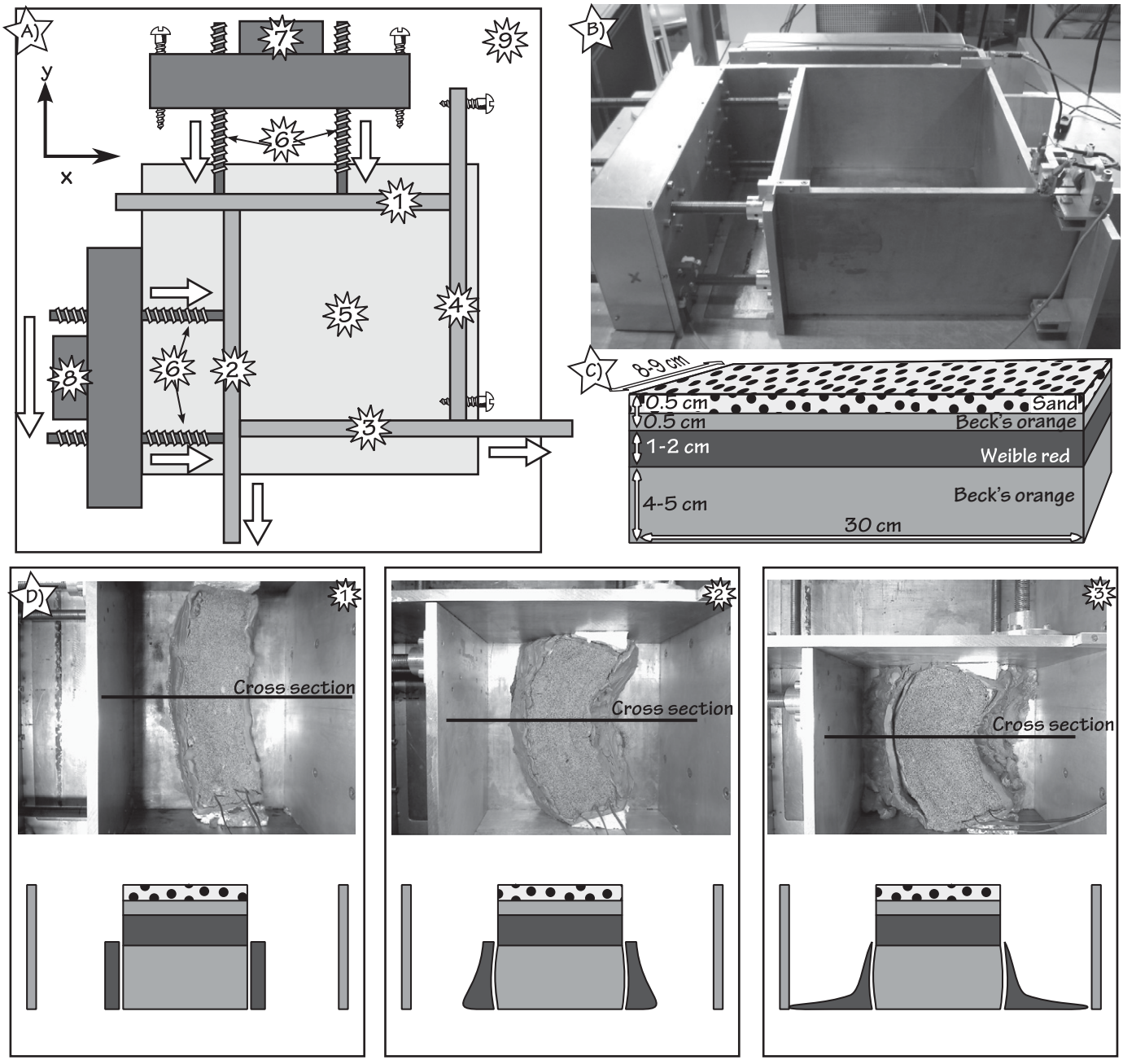

Figure 2. Thermomechanical apparatus at Geozentrum of Frankfurt University. (A) Plan view showing the kinematic framework. 1 and 2—aluminum movable plates in *y* and *x* direction, respectively; 3—movable passive plate; 4—fixed plate; 5—thermal copper plate; 6—worm gears; 7—fixed motor; 8—movable motor in *y* direction; 9—table. (B) Photograph showing the thermomechanical apparatus. (C) Cartoon showing the dimensions and the layering of the experimental setup for the orocline buckling models. Models were built with a 4–5-cm-thick asthenosphere layer made with Beck's orange plasticine, a 1 cm, 1.5 cm, or 2 cm Weible red plasticine mantle lithosphere layer, and a 1 cm crust divided into a 0.5 cm Beck's orange plasticine lower-crust layer and a 0.5 cm upper crust represented by sand. (D) Top view and cross section of experiment Ob10 depicting (1) first stage of the experiment, (2) middle stage of experiment, and (3) final stage.

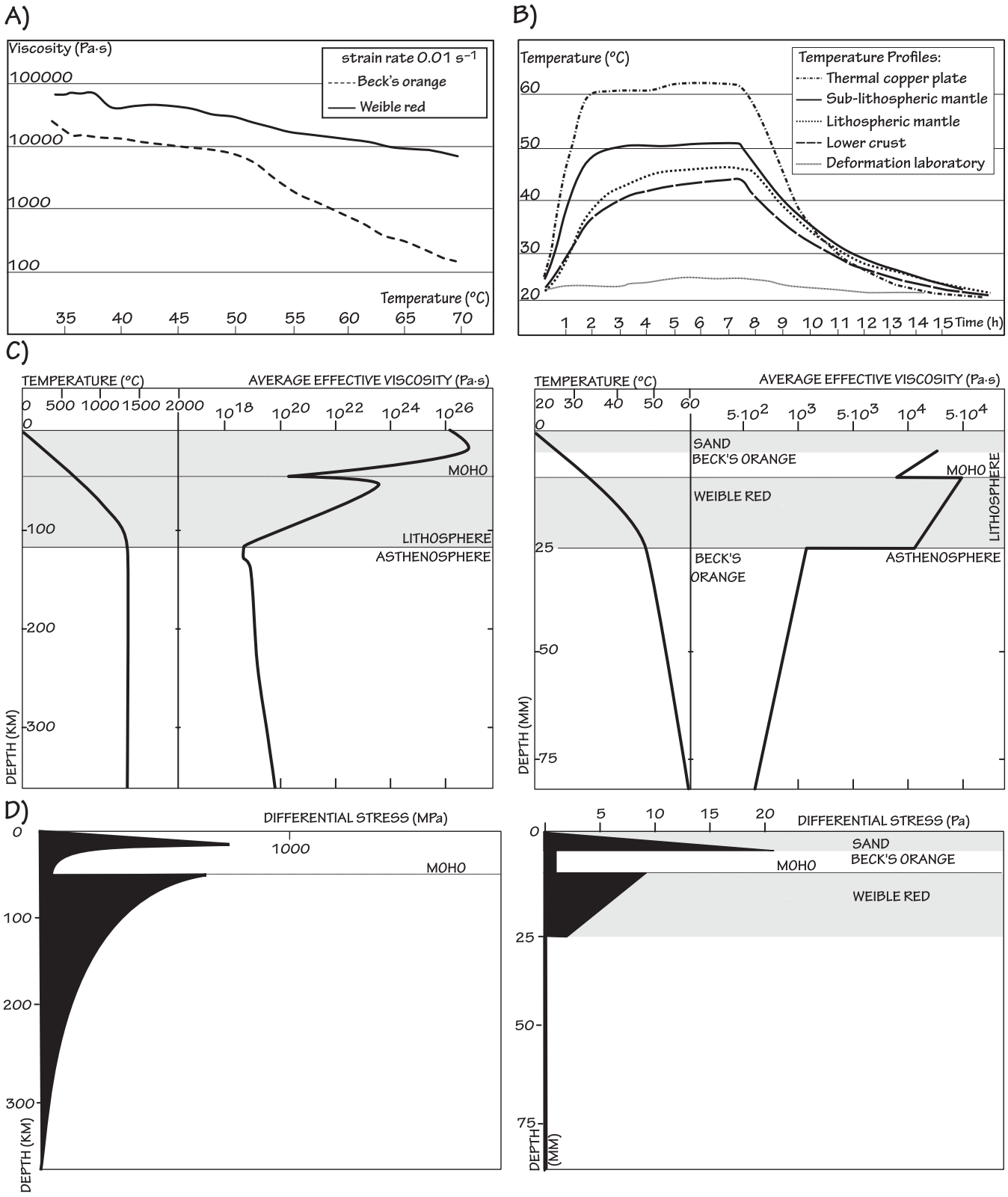

Figure 3. (A) Results of thermo-viscosity tests on Beck's orange and Weible red plasticines at a constant strain rate $\dot{E} = 0.01\ s^{-1}$, similar to the strain rates used in the experiments (modified from Tkalcec, 2010). (B) Example of thermal profile obtained during orocline buckling experiment Ob6. The actual experiment lasted 5 h, between 2 h (time allowed for the sample to acquire the needed temperature) to 7 h (once the experiment had ended). (C) Simplified effective viscosity and temperature profiles for nature and orocline buckling experiment. (D) Simplified strength profiles for the lithosphere and upper asthenosphere of the Earth and for the model.

TABLE 2. SCALING PARAMETERS BETWEEN EXPERIMENTS AND NATURE

		Lower crust	Lithospheric mantle	Asthenosphere
ρ (kg/m³)	Experiment	1250	1400	1250
	Nature	3100	3360	3100
	Scaling factor	0.4	0.41	0.4
η_{eff} (Pa·s)	Experiment	12,900	57,300	590
	Nature	1.13×10^{21}	5×10^{21}	5.15×10^{19}
	Scaling factor	1.146×10^{-17}	1.146×10^{-17}	1.146×10^{-17}
n	Experiment	7.8	4.37	3.41
	Nature	From 4 to 8	From 2 to 5	From 2 to 5

Model Setup

The model's length was limited by the dimension of the apparatus, and this was the main constraint on designing the laboratory experiment (Fig. 2A). The length scale of the models was set at l_m = 30 cm; the length of the Iberian-Armorican Arc around its neutral fiber is $l_n \approx$ 1300 km, which gives a length scale ratio $L^* = l_m/l_n = 2.3 \times 10^{-7}$. Based on this scale and the approximate width of the Iberian-Armorican Arc, which is $W_n \approx$ 350–400 km, the model's width was chosen to be W_m = 8–9 cm. Because there are no constraints on the initial thickness of the lithospheric mantle, three different thicknesses of the model lithospheric mantle (Ml_m = 1.0, 1.5, 2.0 cm) were tested in order to analyze their impact on the style of oroclinal buckling, using the same scaling factor, to represent mantle lithospheric thicknesses of 40, 60, and 80 km. The crust was offset at the same starting thickness in every model, consisting of an upper crust, Uc_m = 0.5 cm, and a lower crust, Lc_m = 0.5 cm, which together represent a slightly thickened continental crust after orogenic shortening (~40 km in nature). We ran our experiments under natural gravity, so the gravity scale ratio is $G^* = G_m/G_n = 1$. Thus, the calculated stress ratio is $\sigma^* = P^*L^*G^* \approx 1^*10^{-7}$; the time scale ratio for the experiments can now be defined as $T^* = M^*/P^*L^*G^* = t_m/t_n \approx 1.2 \times 10^{-10}$; a strain rate ratio is given by $\dot{E}^* = \sigma/M = 8.7 \times 10^9$; and a velocity ratio is given by $V^* = \dot{E}^*L^* \approx 2 \times 10^3$.

We suggest a strain rate for the Iberian-Armorican Arc of ~2×10^{-15} s^{-1} based on the N-S shortening (~900 km) and the time taken for this process (~10 m.y., following the hypothesis of Weil et al. [2010] and Pastor-Galán et al. [2011]). The velocity of the plates was set between 1.5 and 3.5 cm/h, which, considering a shortening of ~15 cm of the initial length of models, made experiments 5 h and 10 h in duration. The strain rate used to run the buckling experiments varied from 1×10^{-5} to 5×10^{-5} s^{-1}. These parameters make a real scale of time (T) between 5×10^{-11} and 1×10^{-10}; velocity (V) between 1.46×10^3 and 3.4×10^3; and strain rate ($\dot{E}$) between 5×10^9 and 2.5×10^{10}, which are consistent with the other scaling parameters.

Boundary Conditions

The copper plate at the base of the apparatus is the lower boundary, acts as a rigid body, and limits the downward development of the model. This copper plate was coated in petroleum jelly that is immiscible with Beck's orange plasticine to minimize slip of the branches of the experiments during the buckling process. The upper boundary is a free surface (Fig. 2D). All models were coated with a 1-cm-thick wall of Weible red plasticine around the Beck's orange bottom layer (experimental asthenosphere) in order to prevent lateral escape of the Beck's orange plasticine, which behaves in a very ductile manner at the temperatures used in the experiments (Fig. 2D). This wall was kinematically independent of the Weible red layer representing the lithospheric mantle and Beck's orange and sand layers representing the crust. The wall was removed from the model before computer tomography was applied. The wall acted as a side boundary for the asthenosphere layer, whereas the lithosphere and crust side boundaries were free. During the experiments, the lower parts of these walls melted and spread because Weible red plasticine can blend with the petroleum jelly, dramatically changing its viscosity. Although the spreading plasticine sometimes touched the side plates (Fig. 2D, part 3), their contact had no influence on the development of the deformation of the layers. Most of the models (except Ob6 and Ob7) were run with small wedges at their ends, which triggered the model to bend around a vertical axis and not to develop a train of horizontal folds (white blocks, Fig. 2D).

Strength and viscosity profiles for the model lithosphere compared with a three-layer lithosphere Earth strength profile (Davy and Cobbold, 1991) are shown in Figure 3D. Ductile strength values were computed for effective viscosities assuming a strain rate of 1×10^{-5} s^{-1}, which is a reasonable approximation of deformation rates observed in the experiments. The strength profile for the sand crust was calculated following Navier-Coulomb and Byerlee laws. The effective strength of the ductile crust, lithospheric mantle, and asthenosphere will vary in the experiments because of variations in the strain rate and the thermal evolution of the plasticines.

The progress in deformation was monitored by digital plan-view photography (Fig. 2D). Digital photographs were taken every minute, resulting in 24 frames per second videos accelerated to 24 min per second (see GSA Data Repository[1]). The temperature was recorded by an electronic logger consisting of four sensors situated in each layer, at one side of the model.

Computer Tomography

Geometrical data of the deformed models can be obtained in two ways. (1) One can slice them mechanically and reconstruct the 3-D interior geometry of the different layers, in which case the model is destroyed. (2) Alternatively, the models can be analyzed using computed tomography (CT), which is a nondestructive imaging technique that is sensitive to the different densities of the materials used (Zulauf et al., 2003).

CT is capable of recording high-resolution 3-D information in a series of 2-D slices (e.g., Colletta et al., 1991) and is extremely appropriate for imaging the models produced with plasticine of different densities (Zulauf et al., 2003). The final models were examined using a multislice spiral CT scanner (Phillips CT brilliance 6 slice). The resulting 3-D images were used to study the different lithospheric mantle morphologies acquired after orocline buckling. Only one model was sliced after applying a CT scan (Fig. 4, Ob1). The CT images were represented in virtual reality .wrl files using the software SMOOTH developed at Geozentrum of Frankfurt University. These files have been transformed into enhanced PDFs, which are more accessible to regular users, and are stored in the GSA Data Repository (see footnote 1).

RESULTS

To a first order, the results obtained from all 14 experiments show consistent results and are summarized in Table 3. After the model had undergone shortening, in each experiment, including those not equipped with wedges at their ends, the initially rectilinear models that simulate a linear orogen buckled around a vertical rotation axis, acquiring an arcuate or horseshoe shape. In geological terms, regardless of differences in thicknesses of the layers or in the strain rate, the model lithospheric mantle was shortened in the core of the orocline and extended in the outer arc.

[1]GSA Data Repository item 2012190, video and virtual reality images of some models,is available at http://www.geosociety.org/pubs/ft2012.htm or by request to editing@geosociety.org.

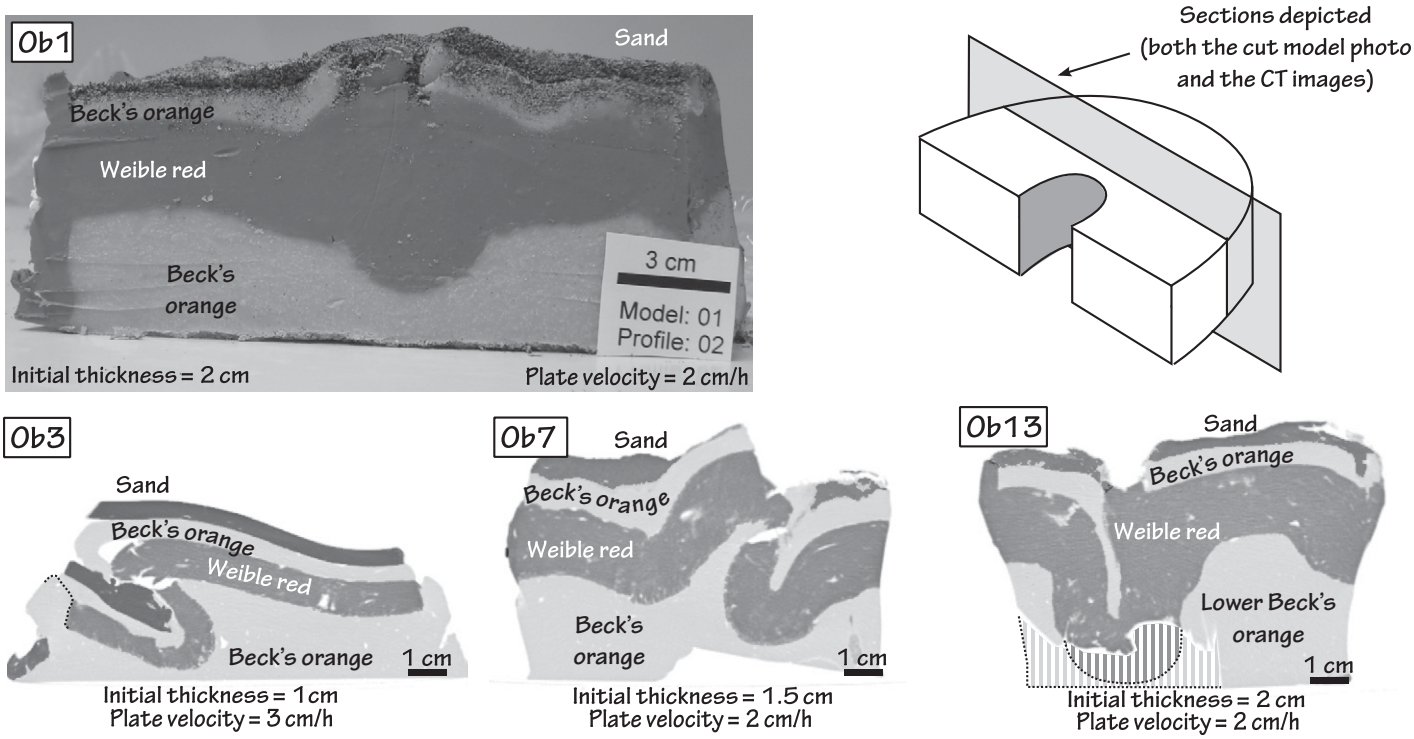

Figure 4. Model cross section and computed tomography sections for orocline buckling models Ob1, Ob3, Ob7, and Ob13, showing the different morphologies of the lithospheric root depending on the initial lithosphere thickness.

In all the experiments, shortening of the inner arc was accompanied by the development of noncylindrical folds causing lithospheric mantle thickening, which resulted in a lithospheric root to the modeled orocline. Lithospheric root development was accompanied by thrusting and duplication of the lower crust (Fig. 4). Every experiment generated a root at least two times, and typically more than 2.5 times, thicker than the original lithospheric mantle. A certain degree of rise of the upper surface of the model over the generated root was recognized in all models. This vertical growth varied from 0.5 to 1.0 cm. On the other hand, the extension in the outer arc was produced through almost radial tensile fractures (e.g., Fig. 5), and so the thickness of the lithospheric mantle in the outer arc was unchanged.

Another feature, present in every experiment, was the growth of tensile fractures parallel to the shortening direction, which crosscut the horseshoe shape of the model (e.g., Fig. 6). These features were developed mainly in the uppermost part of the lithospheric mantle, although they commonly affected the entire layer (hereafter they are termed parallel fractures). Furthermore, most of the experiments showed more or less subvertical shear zones with angles between 30° and 40° with respect to the shortening direction that crosscut the trace of the arc (e.g., Figs. 6, 7, and 8). In three of the experiments (Ob4, Ob9, and Ob14), a shear zone affecting the entire thickness of the model formed (e.g., Fig. 8). In each case, shear zones displaced the growing root, allowing the generation of a new root where the shear zone developed or where its presence inhibited development of the root.

TABLE 3. SYNTHESIS OF THE RESULTS OBTAINED FROM THE OROCLINE BUCKLING EXPERIMENT

Model	Initial mantle lithosphere thickness (cm)	Plate velocity (cm/h)	Root shape	Shear zones	Major tensile fractures
Ob4	1	1	Recumbent fold	Large	12
Ob12	1	2	Recumbent fold	Not identified	14
Ob3	1	3	Recumbent fold	Small	10
Ob2	1.5	1.5	Overturned fold	Small	7
Ob7	1.5	2	Overturned fold	Not identified	7
Ob11	1.5	2	Failed at 30%	–	–
Ob5	1.5	2.2	Overturned fold	Small	6
Ob6	1.5	2.7	Overturned fold	Small	6
Ob1	2	2	Noncylindrical mullions	Not identified	3
Ob8	2	2	Upright fold	Big	4
Ob13	2	2	Upright fold	Small	5
Ob9	2	2.5	Upright fold	Large	4
Ob14	2	2.2	Upright fold	Large	5
Ob10	2	3.5	Upright fold	Small	4

Note: Major tensile fractures refer to tensile fractures that break the entire layer.

Three different geometries—recumbent, overturned, and upright—were produced, depending on the initial lithospheric thickness in the models; these are depicted in Figure 4 and are described in the following paragraphs. The resulting morphologies obtained in the experiments depict the aforementioned folds and shear zones, the geometries of which were dependent essentially on the initial thicknesses of the model lithospheric mantle (Table 3). There was no significant impact of the strain rate or the temperature profiles on the geometry of the deformed samples, although variations of these parameters in the experiments were minor in order to preserve the scaling.

Three experiments were run with an initial model lithospheric mantle thickness (Ml_m) of 1 cm (40 km). The results obtained from these experiments are represented by experiment Ob12

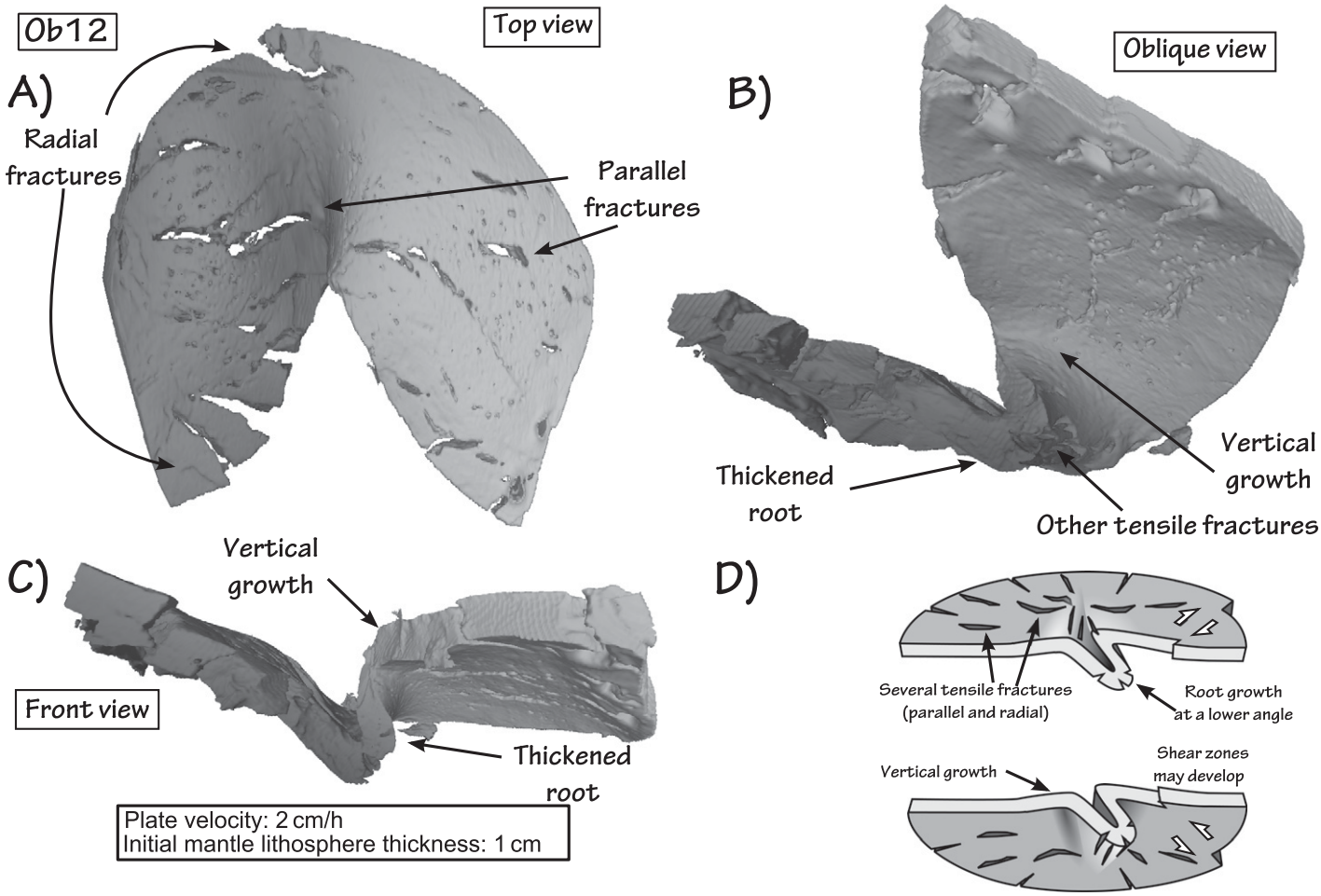

Figure 5. Three-dimensional image of model Ob12 mantle lithosphere layer with 1 cm of initial mantle lithosphere thickness showing the development of an almost recumbent noncylindrical fold as a root and several parallel and radial fractures, from three different views: (A) top view, (B) oblique view, and (C) front view. (D) Conceptual interpretation of the results obtained in model Ob12. Gray scale is a computer pattern designed to improve the visualization of relief when depicted in two dimensions.

(Fig. 5). Models with this thickness developed an almost recumbent, tight-shaped fold with its apex pointing to the outer arc of the experiment, a lithospheric root in the inner arc (Fig. 4, Ob3; Fig. 5C), some radial fractures in the outer arc, and a large number of parallel fractures over the entire layer (Fig. 5B). Although in model Ob12, no oblique shear zones were identified, a small incipient shear zone developed in experiment Ob3, and a longer one developed in model Ob4 (see GSA Data Repository[1]).

Five experiments with an initial model lithospheric mantle thickness of 1.5 cm (60 km) also developed lithospheric roots in the inner arc through tight and overturned folds. In each experiment, the lithospheric mantle in the model was extended in the outer arc by means of radial fractures. Parallel fractures commonly occurred over the entire layer, but they were not as abundant as in the experiments with 1 cm of model mantle lithospheric thickness. Three of the five experiments produced short (<1 cm) shear zones oblique to the compression direction in one of the orocline limbs. Figure 6 shows the most representative experiment of this group (for further images, see GSA Data Repository material[1]).

Finally, the six experiments with an initial model lithospheric mantle thickness of 2 cm acquired two analogous root morphologies: (1) a very tight upright fold (Fig. 4, Ob13; Fig. 7), or (2) a fold train composed of two noncylindrical folds, resembling mullions (Fig. 4, Ob1; for further information, see GSA Data Repository material[1]). Radial fractures occurred in the outer arc, and some parallel fractures developed. Short (<1 cm) shear zones oblique to the compression direction developed in three of the models, and model-scale shear zones developed in two of them.

Three experiments responded to the applied stresses by developing model-scale shear zones. Two of them had an initial model lithospheric mantle thickness (Ml_m) of 2 cm (Ob9 and Ob14) and developed a root shaped as a tight fold. The root of the other model, with Ml_m = 1 cm (Ob4), turned into a recumbent fold. Model Ob14 (Fig. 8) is representative of the morphologies that these models presented, such as an incompletely developed root in the inner arc that is duplicated and off-centered by the effects of the model-size shear zone developed in one of the orocline limbs oblique to the overall shortening direction, and the presence of radial fractures preferentially focused in the outer arc of one limb of the model.

DISCUSSION

Thermomechanical experiments run over scaled lithosphere models produced results that shed light on the processes taking place during the deformation and evolution of the litho-

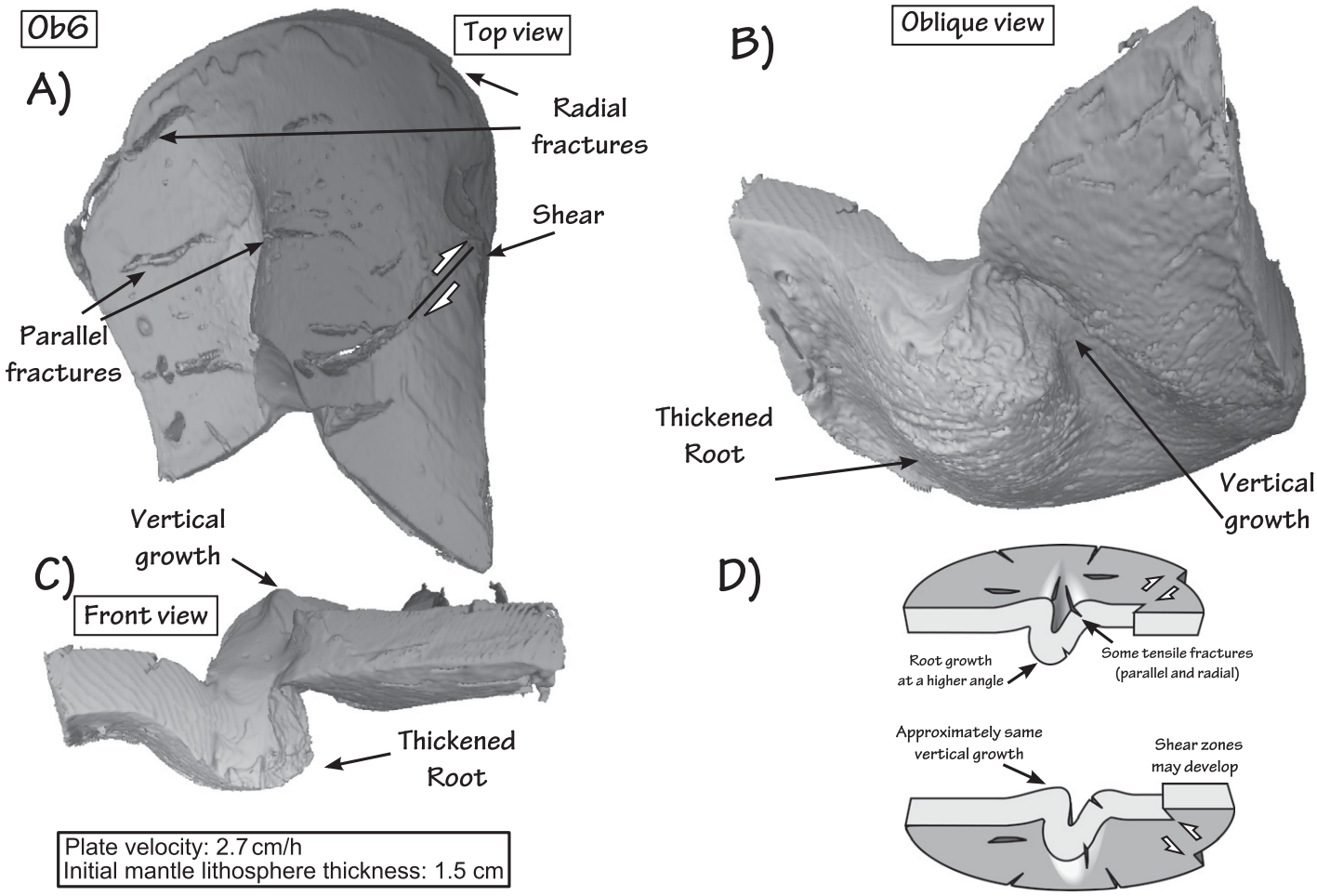

Figure 6. Three-dimensional image of model Ob6 lithosphere with an initial mantle lithosphere thickness of 1.5 cm depicting the development of a noncylindrical overturned fold root and the development of parallel and radial fractures and a small shear zone. Three different views: (A) top view, (B) oblique view, and (C) front view. (D) Conceptual interpretation of the results obtained in model Ob6. Gray scale is a computer pattern designed to improve the visualization of relief when depicted in two dimensions.

spheric mantle related to orocline buckling. In general, the results allow a better understanding of lithospheric-scale processes such as thick-skinned orocline buckling and, in a more particular case, the relationship between orocline development and a lithospheric mantle removal event that is interpreted to have taken place in the late Paleozoic in the Iberian-Armorican Arc. In addition, these experiments show limitations in the development of lithospheric structures due to analogue material behavior, scaling, and laboratory conditions and setup.

Limitations and Interpretation

During the orocline buckling experiments, independently of the initial setup, the strain pattern in the model is characterized by extreme shortening in its core and the generation of a root below the inner arc, as well as by extension in the outer arc developed via extensional fractures. These features were predicted by Ries and Shackleton (1976, their fig. 14-A), who suggested tangential longitudinal strain as the main folding mechanism for lithospheric bending. This mechanism has also been proposed by Gutiérrez-Alonso et al. (2004) to explain the different aforementioned geological effects found in nature, especially in the Iberian-Armorican Arc.

The shapes of the buckled model lithospheric mantle in our experiments are strikingly similar to those obtained in other plate-convergence analogue and numerical models without preexisting subduction (e.g., Pysklywec et al., 2002; Luth et al., 2010), and they depict a marked noncylindrical geometry due to the vertical rotational axis buckling (Pastor-Galán et al., 2012, their figs. 6, 7, 8) instead of a cylindrical one (Shemenda and Grocholsky, 1992; Luth et al., 2010) or an unknown 3-D geometry, like that obtained from 2-D numerical modeling (Arnold et al., 2001; Pysklywec et al., 2002, 2010; Pysklywec, 2006).

A thickened lithospheric root observed in the experiments could trigger lithospheric mantle removal, which would be consistent with the models of Schott and Schmeling (1998), Pysklywec et al. (2002, 2010), Pysklywec (2006), and Morency and Doin (2004), among others. However, neither delamination nor dripping of the lithospheric mantle occurred in the experiments due to the size limitations and the analogue materials used in the experiments, which caused the observed vertical crustal growth over the lithospheric root. The thermal conductivity of plasticine is quite low (between 0.65 and 0.8 $W\ m^{-1}\ K^{-1}$) (Touloukian et al., 1970), which implies that in order to keep a realistic scalable thermal gradient, the sublithospheric mantle in the models could not be thicker than 4 or 5 cm. Hence, the model asthenosphere is not thick enough to avoid the effect of the lower boundary (thermal copper plate)

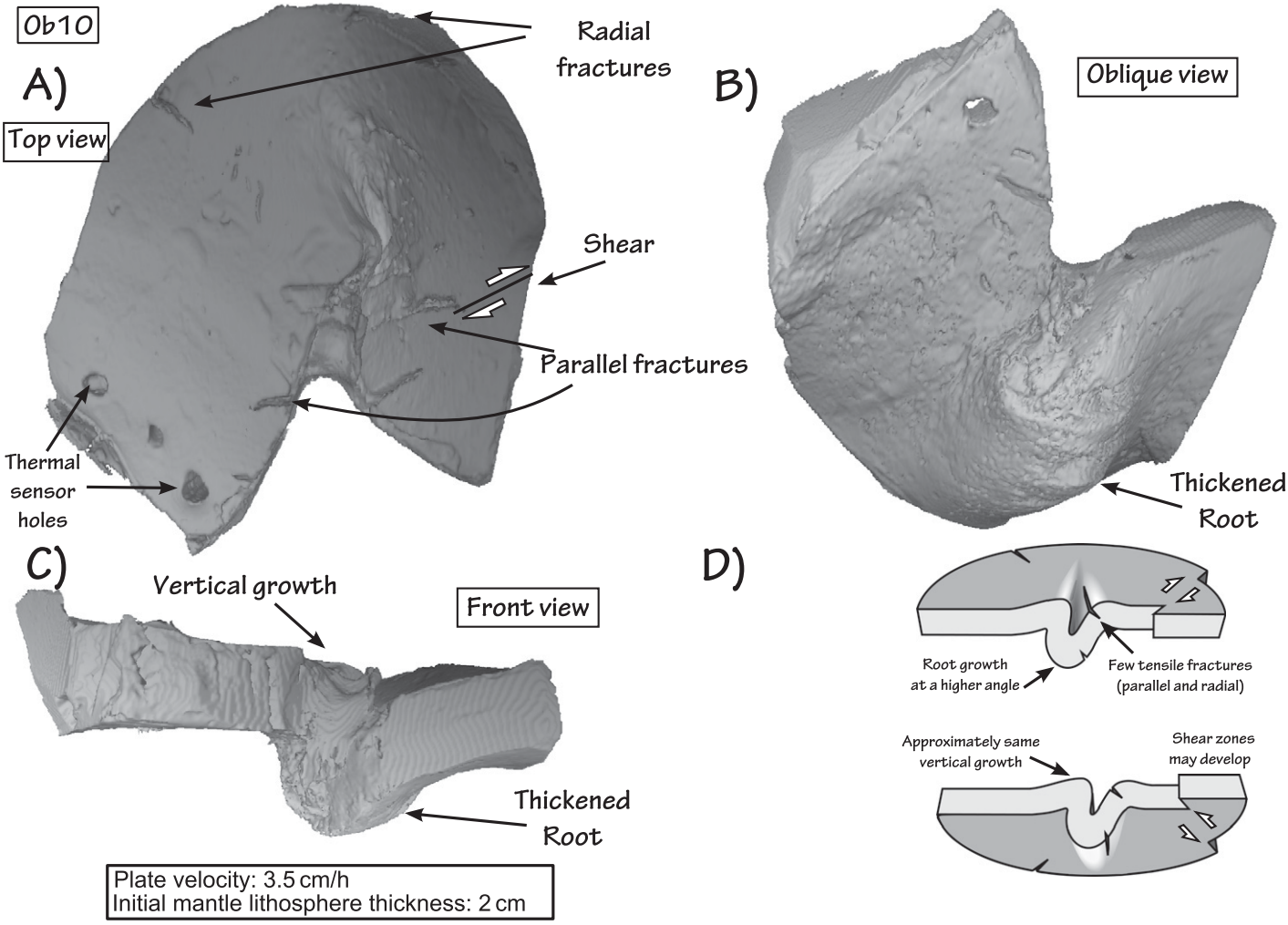

Figure 7. Three-dimensional image of model Ob10 mantle lithosphere with an initial lithosphere thickness of 2 cm showing the development of a slightly overturned root. Few radial and parallel fractures grew up, and a small shear zone can be observed. Three different views: (A) top view, (B) oblique view, and (C) front view. (D) Conceptual interpretation of the results obtained in model Ob10. Gray scale is a computer pattern designed to improve the visualization of relief when depicted in two dimensions.

of the experiments. This lower boundary avoided any further growth, delamination, or dripping of the lithospheric root. Moreover, the yield strength of Beck's orange plasticine is likely too large to let Weible red plasticine detach and sink under natural gravity conditions, at least for the duration of the experiments. The use of a denser plasticine to model the lithospheric mantle would not have modified the results, as the asthenospheric analogue would not have allowed its downward migration. Thus, when the lithospheric mantle could no longer migrate downward, it started to build a positive bulge along the surface of the model. Without the aforementioned experimental limitations, the process in nature would be the opposite: The dynamic sinking of the lithospheric mantle root would pull down the crust above it, resulting in basin formation (Muñoz-Quijano and Gutiérrez-Alonso, 1997a, 1997b).

All of our experiments show extension in the outer arc, mostly produced by radial fractures. This brittle behavior is not expected in natural lithospheric mantle, where deformation should be accommodated by crystal plastic processes (e.g., Karato and Wu, 1993). The development of fractures in the model mantle lithosphere, instead of viscous stretching, could be due to the plastic failure of the materials. In this way, the curvature in the outer arc becomes more pronounced, causing mode 1 tensile fractures in the model lithospheric mantle. Moreover, in nature, there is a considerable confining pressure at depth, which discourages brittle and plastic failure.

Apart from the radial fractures, the growth of tensile fractures observed in the model lithospheric mantle was not expected, as these are not likely to occur in the natural lithospheric mantle. The parallel fractures developed, maintaining the scaling relationship between the initial lithospheric thickness of the model and the spacing of the fractures as found in other natural examples of brittle rocks (e.g., Narr and Suppe, 1991; Mandal et al., 1994; Gross et al., 1995). Enhanced dilatancy due to the lack of confining pressure and, subsequently, plastic failure of the material are probably the most important reasons why these mode 1 tensile axial loading fractures developed in the model lithospheric mantle.

Oblique shear zones (mode 2 fractures) are lacking in every model, and just three of the models display model-scale vertical shear zones that control the final morphology of the model lithospheric mantle. All shear zones developed with angles <40° with respect to the principal shortening direction. Zulauf and Zulauf (2004) documented that in models undergoing high

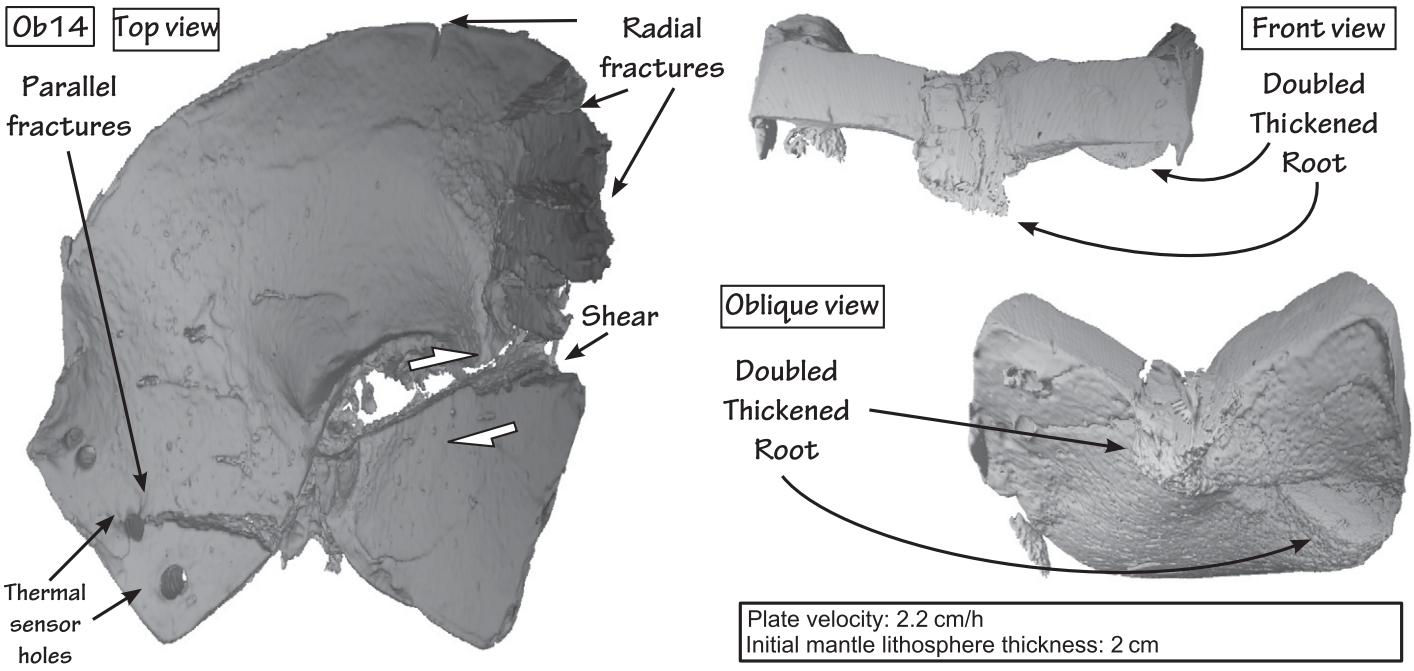

Figure 8. Three-dimensional image of model Ob14 mantle lithosphere showing the development of a large shear zone, which interfered with the growing of the root. See text for explanation.

strain rates ($\dot{E} > 10^{-3}$ s^{-1}), plasticine is not a suitable analogue for viscously deforming rocks because strain tends to be localized along discrete shear corridors in the plasticine. The orocline buckling experiments of the present study were run under lower strain rates ($\dot{E} = 10^{-5}$ s^{-1}), and, despite the local higher strain rates that take place especially in the outer arc of the model, the shear zones of the models mimic natural shear zones observed in most curved orogenic belts. These shear zones are interpreted to develop at the same time as curvature generation (Gutiérrez-Alonso et al., 2010). However, lithospheric-scale shear zones, like those of models Ob4, Ob9, and Ob14 (Fig. 8; GSA Data Repository material [see footnote 1]), which act as high-strain domains, are not easily recognized in nature, although a more distributed pattern of shear zones likely to occur at lithospheric scale can be recognized (e.g., lithospheric-scale shear zones in the North Armorican massifs, Porto-Tomar shear zone; Gutiérrez-Alonso et al., 2010). In our opinion, the lithospheric-scale shear zones probably formed in order to accommodate the lithospheric buckling, but they initiated along the previously formed radial or parallel fractures (see GSA Data Repository material[1]).

Another limitation is the impossibility of measuring the temperature in the growing root, which was presumably higher than the temperature measured at the side of the model because the root is closer to the thermal plate. It would have been useful to know this temperature in order to compare it with numerical and field data, because the mechanism of lithospheric thickening in nature leads to an increase in heat flow, raising the mantle isotherms. The increasing thermal flow drives the chemical and physical process that can trigger lithospheric mantle removal (Leech, 2001).

Implications of the Experimental Results on the Development of the Iberian-Armorican Arc

The new experimental results also improve our understanding of lithospheric mantle behavior during thick-skinned orocline buckling and the dynamics of the Iberian-Armorican Arc. Results and structures obtained from the models here, which produced in all cases a lithospheric root, are in agreement with the structural, petrological, paleomagnetic, and geochronological data described from the Iberian-Armorican Arc.

The main observed differences in the shape of the lithospheric root come from the initial mantle lithospheric thickness, as stated previously. Because there is no possibility to determine the Variscan lithospheric mantle thickness in the Pennsylvanian, we cannot argue which of the results best matches reality. In any case, all the obtained results produced a lithospheric root that was susceptible to subsequent detachment and foundering into the asthenospheric mantle (Pysklywec and Cruden, 2004). From this point of view, we can link the experiments to the geological observations in the Iberian-Armorican Arc.

An interpretation of the whole process of thick-skinned orocline buckling and the possible subsequent delamination or dripping of the lithospheric root inferred from structural, petrological, and geochemical studies (Fernández-Suárez et al., 2000; Gutiérrez-Alonso et al., 2004, 2011a, 2011b), based on the results of the experiments produced in this work and on the aforementioned geological criteria, is depicted in Figure 9. For our interpretation, we have chosen the case where the lithospheric mantle had an intermediate thickness (~60 km), which is plausible within a postorogenic environment. In any case, all models produced a lithospheric root than can be correlated to the one inferred from the geological data.

Using the modeling results and the geological constraints, we propose that during orocline development, the effect of mechanical thinning in the outer arc (Fig. 9) caused the upwelling of the asthenosphere and the accompanying thermal uplift (Muñoz-Quijano and Gutiérrez-Alonso, 2007a, 2007b) due to the increased heat flow and the subsequent lower-crustal melting, which is supported by the emplacement of early post-tectonic granitoids at ca. 310–300 Ma (Fernández-Suárez et al., 2000; Gutiérrez-Alonso et al., 2011a, 2011b). In the upper crust, this extension was accommodated by slip along crustal-scale shear zones (Gutiérrez Alonso

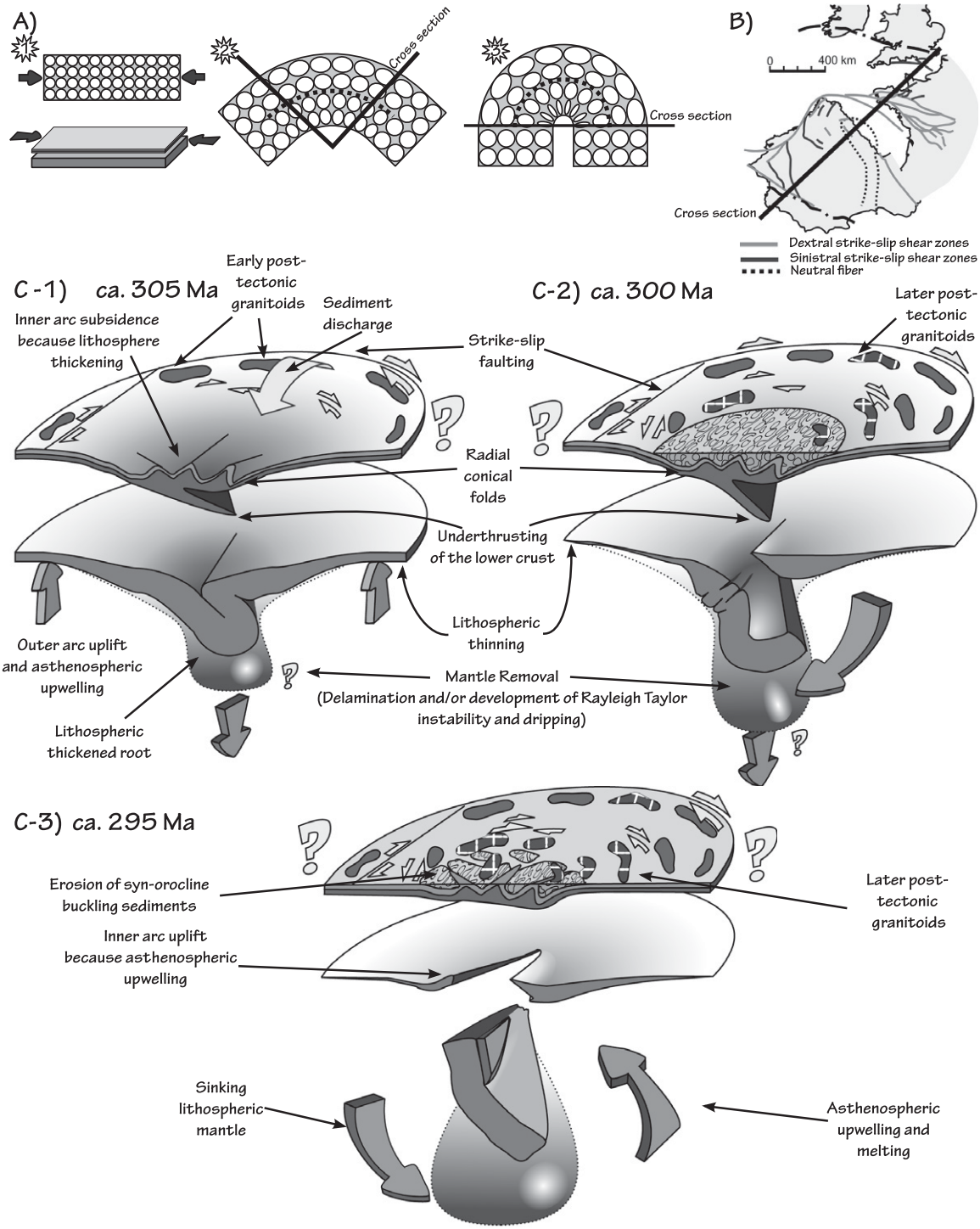

Figure 9. Cartoon depicting the proposed interpretation for the Iberian-Armorican Arc lithospheric development during and after orocline buckling. (A) 1—Sketch showing an ideal initial stage of a linear or nearly linear Variscan belt and its plan view; 2—plan view of the effects at middle stage of the orocline buckling based on the deformation mechanism proposed (longitudinal tangential strain) showing a cross section that corresponds to the C-1 block diagram; (3) plan view of the final stage of orocline buckling displaying a cross section that is represented in C-2 block diagram. (B) Map view of the final stage of Iberian-Armorican Arc after lithospheric delamination and/or dripping but before the opening of the Bay of Biscay, showing a cross section that corresponds to block diagram C-3. (C) 1—Simplified block diagram of the Iberian-Armorican Arc at ca. 305 Ma showing stretching in the outer arc and thickening in the inner arc. 2—Block diagram showing the effects of orocline buckling at ca. 300 Ma. The growth of the root created a basin in the core of the arc, and this lithospheric root became unstable and began to break. 3—Block diagram showing the final stage of delamination and/or dripping with the replacement of the mantle lithosphere by upwelling asthenosphere.

et al., 2010). In contrast, the shortening in the core of the arc produced a thickened mantle lithospheric root and lower-crust duplication by means of underthrusting, independently of the lithospheric mantle initial thickness. Collectively, these processes caused the depression of the core, which resulted in sediment discharge into the core of the arc (Gutiérrez-Alonso et al., 2004) and marine strata as the vestiges of a relict epicontinental sea (Merino-Tomé et al., 2009). In the upper crust, this shortening was accommodated by radial conical folding (Julivert and Marcos, 1973; Gutiérrez-Alonso, 1992; Aller and Gallastegui, 1995; Pastor-Galán et al., 2012), reverse and strike-slip faulting (Alonso, 1989; Nijman and Savage, 1989), and out-of-sequence thrusting (Alonso et al., 2009). The shear zones developed in the models at angles <40° to the compression direction are consistent with the geometry and kinematics of some of the shear zones that cut the Iberian-Armorican Arc's trace (Gutiérrez-Alonso et al., 2010).

The mass imbalance between the thickened root beneath the inner arc and the stretched lithospheric mantle beneath the outer arc presumably caused an important gravitational instability that brought about the detachment and removal of the lithospheric root, which would have permitted the asthenosphere to invade the location occupied by the former lithosphere (Pysklywec et al., 2010). The foundering of the sinking root further stretched the lithospheric mantle and probably dragged down part of the remaining, previously thinned outer arc lithospheric mantle, causing the final asthenospheric upwelling. Evidence for this final substitution of the lithospheric mantle by the asthenosphere is recorded by the contrast in the Sm/Nd isotopic signature observed in mantle-derived rocks that predate and postdate the postulated lithospheric mantle removal event (Gutiérrez-Alonso et al., 2011a). The enhanced thermal activity caused a widespread thermal event from 310 to 300 Ma in the hinterland and from 300 to 285 Ma in the foreland fold-and-thrust belt (Valverde-Vaquero, 1992; Fernández-Suárez et al., 2000; Gutiérrez-Alonso et al., 2011b; Fernández-Suárez, 1994; Martínez and Rolet, 1988; Martín-Izard et al., 2000; Colmenero et al., 2008; Gasparrini et al., 2003).

The duration of orocline formation and the subsequent lithospheric mantle removal lasted ~10 m.y., based on geological data (Weil et al., 2010), starting at ca. 310 Ma to ca. 300 Ma (Pastor-Galán et al., 2011) (Pennsylvanian). Lithospheric mantle removal, inferred from the igneous activity in the inner arc, which corresponds to the foreland fold-and-thrust belt, seems to have started at ca. 300 Ma (Gutiérrez-Alonso et al., 2011b), when the root was thick enough (Schott and Schmeling, 1998) to destabilize and founder. The lithospheric mantle removal would have lasted between 5 and 10 m.y., according to numerical models (Schott and Schmeling, 1998; Pysklywec et al., 2010), and the related magmatic activity lasted for ~15 m.y. (Gutiérrez-Alonso et al., 2008).

These data imply that Iberian-Armorican Arc formation was a relatively fast lithospheric-scale tectonic process, with bulk north-south shortening acting at shortening rates between 5 and 10 cm/yr. Such large, continuous, and rapid thick-skinned processes could be explained in the context of large-scale plate motions as in the scenario proposed by Gutiérrez-Alonso et al. (2008) for Iberian-Armorican Arc buckling.

CONCLUSIONS

Analogue modeling of orocline buckling has revealed a powerful tool to mimic lithospheric-scale processes similar to those observed in nature. The experiments provided useful insights indicating that during thick-skinned orocline buckling of the lithosphere, tangential longitudinal strain is a plausible mechanism of deformation, causing extension in the outer arc and significant shortening in the inner arc. The extension of the lithospheric mantle in the outer arc is probably accommodated by viscous stretching, whereas extension in the crust is accommodated by crustal-scale shear zones. On the other hand, the inner arc shortening is adjusted in the lithospheric mantle by ductile flow and folding of the lithosphere, developing a well-defined lithospheric root.

Detachment and removal of the lithospheric mantle thickened root were not observed due to experimental limitations. However, according to other modeling in the literature (e.g., Schott and Schmeling, 1998; Morency and Doin, 2004), it is expected that such a lithospheric thickened root would delaminate or drip. This process is likely to be responsible for the anomalous thermal activity recorded in the Iberian-Armorican Arc. Further experiments are required with different scaling and materials in order to permit mantle removal.

ACKNOWLEDGMENTS

This paper is part of the International Geological Correlation Programme (IGCP) projects 574 and 597. Gutiérrez-Alonso and Pastor-Galán were funded by ODRE II research project CGL2009-1367 ("Oroclines and Delamination: Relations and Effects"), from the Spanish Ministry of Science and Innovation. Pastor-Galán was also funded by an Ayuda para la Contratación del Personal Investigador grant from the Junta de Castilla and Leon and a Suvención Obtención Mención Europea grant from the Spanish Ministry of Education. We acknowledge financial support from the Deutsche Forschungsgemeinschaft (DFG) for thermomechanical apparatus and analogue material (grant Zu 73/13). We thank Mark Peinl for his help with the 3-D software. Brendan Murphy, Andrew Hynes, and two anonymous reviewers contributed to improving the manuscript.

REFERENCES CITED

Aller, J., and Gallastegui, J., 1995, Analysis of kilometric-scale superposed folding in the central coal basin (Cantabrian zone, NW Spain): Journal of Structural Geology, v. 17, no. 7, p. 961–969, doi:10.1016/0191-8141(94)00115-G.

Allmendinger, R.W., Figueroa, D., Snyder, D., Beer, J., Mpodozis, C., and Isacks, B.L., 1990, Foreland shortening and crustal balancing in the Andes at 30°S latitude: Tectonics, v. 9, no. 4, p. 789–809, doi:10.1029/TC009i004p00789.

Allmendinger, R.W., Jordan, T.E., Kay, S.M., and Isacks, B.L., 1997, The evolution of the Altiplano-Puna Plateau of the central Andes: Annual Review of Earth and Planetary Sciences, v. 25, no. 1, p. 139–174, doi:10.1146/annurev.earth.25.1.139.

Alonso, J.L., 1989, Fold reactivation involving angular unconformable sequences—Theoretical-analysis and natural examples from the Cantabrian Zone, NW Spain: Tectonophysics, v. 170, no. 1–2, p. 57–77, doi:10.1016/0040-1951(89)90103-0.

Alonso, J.L., Marcos, A., and Suárez, A., 2009, Paleogeographic inversion resulting from large out of sequence breaching thrusts: The Leon fault (Cantabrian zone, NW Iberia). A new picture of the external Variscan thrust belt in the Ibero-Armorican Arc: Geologica Acta, v. 7, no. 4, p. 451–473.

Álvarez-Marron, J., and Pérez-Estaún, A., 1988, Thin skinned tectonics in the Ponga region (Cantabrian zone, NW Spain): Geologische Rundschau, v. 77, no. 2, p. 539–550, doi:10.1007/BF01832397.

Arnold, J., Jacoby, W.R., Schmeling, H., and Schott, B., 2001, Continental collision and the dynamic and thermal evolution of the Variscan orogenic crustal root—Numerical models: Journal of Geodynamics, v. 31, no. 3, p. 273–291.

Autin, J., Bellahsen, N., Husson, L., Beslier, M.-O., Leroy, S., and d'Acremont, E., 2010, Analog models of oblique rifting in a cold lithosphere: Tectonics, v. 29, p. TC6016, doi:10.1029/2010TC002671.

Bard, J.P., Capdevila, R., and Matte, P., 1968, La Structure de la Chaine Hercynienne de la Meseta Iberique: Comparison avec les Segments Voisins: Paris, Editions Technip.

Beaumont, C., Jamieson, R.A., Nguyen, M.H., and Lee, B., 2001, Himalayan tectonics explained by extrusion of a low-viscosity crustal channel coupled to focused surface denudation: Nature, v. 414, p. 738–742, doi:10.1038/414738a.

Brun, J.P., and Burg, J.P., 1982, Combined thrusting and wrenching in the Ibero-Armorican Arc—A corner effect during continental collision: Earth and Planetary Science Letters, v. 61, no. 2, p. 319–332, doi:10.1016/0012-821X(82)90063-2.

Burg, J.-P., and Podladchikov, Y., 2000, From buckling to asymmetric folding of the continental lithosphere: Numerical modelling and application to the Himalayan syntaxes, *in* Treloar, P.J., Searle, M.P., Asif Khan, M., and Qasim Jan, M., eds., Tectonics of the Nanga Parbat syntaxis and the Western Himalaya: Geological Society of London Special Publication 170, p. 219–236.

Butler, R.F., Richards, D.R., Sempere, T., and Marshall, L.G., 1995, Paleomagnetic determinations of vertical-axis tectonic rotations from Late Cretaceous and Paleocene strata of Bolivia: Geology, v. 23, no. 9, p. 799–802, doi:10.1130/0091-7613(1995)023<0799:PDOVAT>2.3.CO;2.

Carey, S.W., 1955, The orocline concept in geotectonics: Royal Society of Tasmania Proceedings, v. 89, p. 255–288.

Carter, N.L., and Tsenn, M.C., 1987, Flow properties of continental lithosphere: Tectonophysics, v. 136, no. 1–2, p. 27–63, doi:10.1016/0040-1951(87)90333-7.

Cobbold, P.R., and Jackson, M.P.A., 1992, Gum rosin (colophony): A suitable material for thermomechanical modelling of the lithosphere: Tectonophysics, v. 210, no. 3–4, p. 255–271, doi:10.1016/0040-1951(92)90325-Z.

Colletta, B., Letouzey, J., Pinedo, R., Ballard, J.F., and Bale, P., 1991, Computerized X-ray tomography analysis of sandbox models: Examples of thin-skinned thrust systems: Geology, v. 19, no. 11, p. 1063–1067, doi:10.1130/0091-7613(1991)019<1063:CXRTAO>2.3.CO;2.

Colmenero, J.R., and Prado, J.G., 1993, Coal basins in the Cantabrian Mountains, northwestern Spain: International Journal of Coal Geology, v. 23, no. 1–4, p. 215–229, doi:10.1016/0166-5162(93)90049-G.

Colmenero, J.R., Suárez-Ruiz, I., Fernández-Suárez, J., Barba, P., and Llorens, T., 2008, Genesis and rank distribution of Upper Carboniferous coal basins in the Cantabrian Mountains, northern Spain: International Journal of Coal Geology, v. 76, no. 3, p. 187–204, doi:10.1016/j.coal.2008.08.004.

Copley, A., Avouac, J.-P., and Wernicke, B.P., 2011, Evidence for mechanical coupling and strong Indian lower crust beneath southern Tibet: Nature, v. 472, no. 7341, p. 79–81, doi:10.1038/nature09926.

Cunningham, W.D., 1993, Strike-slip faults in the southernmost Andes and the development of the Patagonian orocline: Tectonics, v. 12, no. 1, p. 169–186, doi:10.1029/92TC01790.

Dallmeyer, R.D., Martínez-Catalán, J.R., Arenas, R., Ibarguchi, J.I.G., Alonso, G.G., Farias, P., Bastida, F., and Aller, J., 1997, Diachronous Variscan tectonothermal activity in the NW Iberian Massif: Evidence from Ar-40/Ar-39 dating of regional fabrics: Tectonophysics, v. 277, no. 4, p. 307–337, doi:10.1016/S0040-1951(97)00035-8.

Davy, Ph., and Cobbold, P., 1988, Indentation tectonics in nature and experiment: Bulletin of the Geological Institute of Uppsala, v. 14, p. 129–141.

Davy, Ph., and Cobbold, P.R., 1991, Experiments on shortening of a 4-layer model of the continental lithosphere: Tectonophysics, v. 188, no. 1–2, p. 1–25, doi:10.1016/0040-1951(91)90311-F.

Dias, R., and Ribeiro, A., 1995, The Ibero-Armorican Arc—A collision effect against an irregular continent: Tectonophysics, v. 246, no. 1–3, p. 113–128, doi:10.1016/0040-1951(94)00253-6.

Dietl, C., and Koyi, H., 2011, Sheets within diapirs—Results of a centrifuge experiment: Journal of Structural Geology, v. 33, no. 1, p. 32–37, doi:10.1016/j.jsg.2010.10.010.

Eaton, D.W., Darbyshire, F., Evans, R.L., Grütter, H., Jones, A.G., and Yuan, X., 2009, The elusive lithosphere-asthenosphere boundary (LAB) beneath cratons: Lithos, v. 109, no. 1–2, p. 1–22, doi:10.1016/j.lithos.2008.05.009.

Eldredge, S., Bachtadse, V., and Van Der Voo, R., 1985, Paleomagnetism and the orocline hypothesis: Tectonophysics, v. 119, no. 1–4, p. 153–179, doi:10.1016/0040-1951(85)90037-X.

Engelder, T., and Geiser, P., 1980, On the use of regional joint sets as trajectories of paleostress fields during the development of the Appalachian plateau, New York: Journal of Geophysical Research, v. 85, p. 6319–6341, doi:10.1029/JB085iB11p06319.

Fernández-Lozano, J., Sokoutis, D., Willingshofer, E., Cloetingh, S., and Vicente, G.D., 2011, Cenozoic deformation of Iberia: A model for intraplate mountain building and basin development based on analogue modeling: Tectonics, v. 30, p. TC1001, doi:10.1029/2010TC002719.

Fernández-Suárez, J., 1994, Petrología de los Granitos Peralumínicos y Metamorfismo de Labanda Boal–Los Ancares [Ph.D. thesis]: Oviedo, Spain, Universidad de Oviedo, 374 p.

Fernández-Suárez, J., Dunning, G.R., Jenner, G.A., and Gutiérrez-Alonso, G., 2000, Variscan collisional magmatism and deformation in NW Iberia: Constraints from U-Pb geochronology of granitoids: Journal of the Geological Society of London, v. 157, p. 565–576, doi:10.1144/jgs.157.3.565.

Fernández-Suárez, J., Gutiérrez-Alonso, G., Johnston, S.T., Jeffries, T.E., Pastor-Galán, D., Jenner, G.A., and Murphy, J.B., 2011, Iberian late-Variscan granitoids: Some considerations on crustal sources and the significance of "mantle extraction ages": Lithos, v. 123, no. 1–4, p. 121–132, doi:10.1016/j.lithos.2010.09.010.

Ferrill, D.A., and Groshong, R.H., Jr., 1993, Kinematic model for the curvature of the northern Subalpine Chain, France: Journal of Structural Geology, v. 15, no. 3–5, p. 523–541.

Freed, A.M., Bürgmann, R., Calais, E., and Freymueller, J., 2006, Stress-dependent power-law flow in the upper mantle following the 2002 Denali, Alaska, earthquake: Earth and Planetary Science Letters, v. 252, no. 3–4, p. 481–489, doi:10.1016/j.epsl.2006.10.011.

Gasparrini, M., Bakker, R.J., Bechstadt, T., and Boni, M., 2003, Hot dolomites in a Variscan foreland belt: Hydrothermal flow in the Cantabrian zone (NW Spain): Journal of Geochemical Exploration, v. 78–79, p. 501–507, doi:10.1016/S0375-6742(03)00115-8.

Ghosh, S.K., Khan, D., and Sengupta, S., 1995, Interfering folds in constrictional deformation: Journal of Structural Geology, v. 17, p. 1361–1373, doi:10.1016/0191-8141(95)00027-B.

Gray, M.B., and Stamatakos, J., 1997, New model for evolution of fold and thrust belt curvature based on integrated structural and paleomagnetic results from the Pennsylvania salient: Geology, v. 25, p. 1067–1070, doi:10.1130/0091-7613(1997)025<1067:NMFEOF>2.3.CO;2.

Gross, M.R., Fischer, M.P., Engelder, T., and Greenfield, R.J., 1995, Factors controlling joint spacing in interbedded sedimentary rocks: Integrating numerical models with field observations from the Monterey Formation, USA, *in* Ameen, M.S., ed., Fractography: Fracture Topography as a Tool in Fracture Mechanics and Stress Analysis: Geological Society of London Special Publication 92, p. 215–233.

Grubbs, K., and van der Voo, R., 1976, Structural deformation of the Idaho-Wyoming overthrust belt (U.S.A.), as determined by Triassic paleomagnetism: Tectonophysics, v. 33, no. 3–4, p. 321–336, doi:10.1016/0040-1951(76)90151-7.

Gutiérrez-Alonso, G., 1992, El Antiforme del Narcea y su Relación con los Mantos Occidentales de la Zona Cantábrica [Ph.D. thesis]: Oviedo, Spain, Universidad de Oviedo, 317 p.

Gutiérrez-Alonso, G., Fernández-Suárez, J., and Weil, A.B., 2004, Orocline triggered lithospheric delamination, *in* Sussman, A., and Weil, A.B., eds., Orogenic Curvature: Integrating Paleomagnetic and Structural Analysis: Geological Society of America Special Paper 383, p. 121–131.

Gutiérrez-Alonso, G., Fernández-Suárez, J., Weil, A.B., Murphy, J.B., Nance, R.D., Corfu, F., and Johnston, S.T., 2008, Self-subduction of the Pangaean global plate: Nature Geoscience, v. 1, no. 8, p. 549–553, doi:10.1038/ngeo250.

Gutiérrez-Alonso, G., Fernández-Suárez, J., Jeffries, T., Collins, A.S., Johnston, S.T., González-Clavijo, E., and Pastor-Galán, D., 2010, Delimitação mediante idades absolutas ($^{40}Ar^{*}$-^{39}Ar e U-Pb) dodesenvolvimento oroclinal e da delaminação litosférica associada no Arco Ibero Armoricano: Revista Electrónica de Ciências da Terra, v. 23–4.

Gutiérrez-Alonso, G., Murphy, J.B., Fernández-Suárez, J., Weil, A.B., Franco, M.P., and Gonzalo, J.C., 2011a, Lithospheric delamination in the core of Pangea: Sm-Nd insights from the Iberian mantle: Geology, v. 39, no. 2, p. 155–158, doi:10.1130/G31468.1.

Gutiérrez-Alonso, G., Fernández-Suárez, J., Jeffries, T.E., Johnston, S.T., Pastor-Galán, D., Murphy, J.B., González, M.P.F., and Gonzalo, J.C., 2011b, Diachronous post-orogenic magmatism within a developing orocline in Iberia, European Variscides: Tectonics, v. 30, TC5008, doi:10.1029/2010TC002845.

Hirt, A.M., Lowrie, W., Julivert, M., and Arboleya, M.L., 1992, Paleomagnetic results in support of a model for the origin of the Asturian arc: Tectonophysics, v. 213, no. 3–4, p. 321–339, doi:10.1016/0040-1951(92)90461-E.

Hirth, G., Teyssier, C., and Dunlap, J., 2001, An evaluation of quartzite flow laws based on comparisons between experimentally and naturally deformed rocks: International Journal of Earth Sciences, v. 90, no. 1, p. 77–87, doi:10.1007/s005310000152.

Houseman, G.A., McKenzie, D.P., and Molnar, P., 1981, Convective instability of a thickened boundary layer and its relevance for the thermal evolution of continental convergent belts: Journal of Geophysical Research, v. 86, p. 6115–6132, doi:10.1029/JB086iB07p06115.

Hubbert, M.K., 1937, Theory of scale models as applied to the study of geologic structures: Geological Society of America Bulletin, v. 48, p. 1459–1519.

Irving, E., and Opdyke, N.D., 1965, The palaeomagnetism of the Bloomsburg Red Beds and its possible application to the tectonic history of the Appalachians: Geophysical Journal of the Royal Astronomical Society, v. 9, p. 153–167, doi:10.1111/j.1365-246X.1965.tb02067.x.

Isacks, B.L., 1988, Uplift of the central Andean plateau and bending of the Bolivian orocline: Journal of Geophysical Research–Solid Earth and Planets, v. 93, no. B4, p. 3211–3231, doi:10.1029/JB093iB04p03211.

Jacobs, J., and Thomas, R.J., 2004, Himalayan-type indenter-escape tectonics model for the southern part of the late Neoproterozoic–early Paleozoic East African–Antarctic orogen: Geology, v. 32, no. 8, p. 721–724, doi:10.1130/G20516.1.

Johnson, K.M., Hilley, G.E., and Bürgmann, R., 2007, Influence of lithosphere viscosity structure on estimates of fault slip rate in the Mojave region of the San Andreas fault system: Journal of Geophysical Research, v. 112, p. B07408, doi:10.1029/2006JB004842.

Johnston, S.T., 2000, The Cape fold belt and syntaxis and the rotated Falkland Islands: Dextral transpressional tectonics along the southwest margin of Gondwana: Journal of African Earth Sciences, v. 31, no. 1, p. 51–63, doi:10.1016/S0899-5362(00)00072-5.

Johnston, S.T., 2001, The Great Alaskan terrane wreck: Reconciliation of paleomagnetic and geological data in the northern Cordillera: Earth and Planetary Science Letters, v. 193, no. 3–4, p. 259–272, doi:10.1016/S0012-821X(01)00516-7.

Julivert, M., 1971, L'évolution structurale de l'Arc Asturien, *in* Histoire Structurale du Golfe de Gascogne: Paris, Editions Technip, Collection Colloques et Séminaires 22, tome 1, p. 12-1–12-28.

Julivert, M., and Arboleya, M.L., 1984, A geometrical and kinematical approach to the nappe structure in an arcuate fold belt—The Cantabrian nappes (Hercynian chain, NW Spain): Journal of Structural Geology, v. 6, no. 5, p. 499–519, doi:10.1016/0191-8141(84)90061-0.

Julivert, M., and Arboleya, M.L., 1986, Areal balancing and estimate of areal reduction in a thin-skinned fold-and-thrust belt (Cantabrian zone, NW Spain)—Constraints on its emplacement mechanism: Journal of Structural Geology, v. 8, no. 3–4, p. 407–414, doi:10.1016/0191-8141(86)90059-3.

Julivert, M., and Marcos, A., 1973, Superimposed folding under flexural conditions in Cantabrian zone (Hercyniancordillera, northwest Spain): American Journal of Science, v. 273, no. 5, p. 353–375, doi:10.2475/ajs.273.5.353.

Karato, S., and Wu, P., 1993, Rheology of the upper mantle: A synthesis: Science, v. 260, no. 5109, p. 771–778, doi:10.1126/science.260.5109.771.

Keep, M., 2000, Models of lithospheric-scale deformation during plate collision: Effects of indentor shape and lithospheric thickness: Tectonophysics, v. 326, no. 3–4, p. 203–216, doi:10.1016/S0040-1951(00)00123-2.

Kollmeier, J.M., van der Pluijm, B.A., and Van der Voo, R., 2000, Analysis of Variscan dynamics; early bending of the Cantabria-Asturias Arc, northern Spain: Earth and Planetary Science Letters, v. 181, no. 1–2, p. 203–216, doi:10.1016/S0012-821X(00)00203-X.

Lash, G.G., 1988, Along-strike variations in foreland basin evolution: Possible evidence for continental collision along an irregular margin: Basin Research, v. 1, no. 2, p. 71–83, doi:10.1111/j.1365-2117.1988.tb00006.x.

Lawrence, R.D., Yeats, R.S., Khan, S.H., Farah, A., and DeJong, K.A., 1981, Thrust and strike slip fault interaction along the Chaman transform zone, Pakistan, *in* McClay, K.R., and Price, N.J., eds., Thrust and Nappe Tectonics: Geological Society of London Special Publication 9, p. 363–370.

Leech, M.L., 2001, Arrested orogenic development: Eclogitization, delamination, and tectonic collapse: Earth and Planetary Science Letters, v. 185, no. 1–2, p. 149–159, doi:10.1016/S0012-821X(00)00374-5.

Lefort, J.-P., 1979, Iberian-Armorican Arc and Hercynian orogeny in western Europe: Geology, v. 7, no. 8, p. 384–388, doi:10.1130/0091-7613(1979)7<384:IAAHOI>2.0.CO;2.

Luth, S., Willingshofer, E., Sokoutis, D., and Cloetingh, S., 2010, Analogue modelling of continental collision: Influence of plate coupling on mantle lithosphere subduction, crustal deformation and surface topography: Tectonophysics, v. 484, no. 1–4, p. 87–102, doi:10.1016/j.tecto.2009.08.043.

MacDonald, W.D., 1980, Net tectonic rotation, apparent tectonic rotation, and the structural tilt correction in paleomagnetic studies: Journal of Geophysical Research, v. 85, no. B7, p. 3659–3669, doi:10.1029/JB085iB07p03659.

Maffione, M., Speranza, F., and Faccenna, C., 2009, Bending of the Bolivian orocline and growth of the central Andean Plateau: Paleomagnetic and structural constraints from the Eastern Cordillera (22–24°S, NW Argentina): Tectonics, v. 28, p. TC4006, doi:10.1029/2008TC002402.

Malavieille, J., 2010, Impact of erosion, sedimentation, and structural heritage on the structure and kinematics of orogenic wedges: Analog models and case studies: GSA Today, v. 20, no. 1, p. 4–10, doi:10.1130/GSATG48A.1.

Mandal, N., Deb, S.K., and Khan, D., 1994, Evidence for a nonlinear relationship between fracture spacing and layer thickness: Journal of Structural Geology, v. 16, no. 9, p. 1275–1281, doi:10.1016/0191-8141(94)90069-8.

Marques, F.O., Mateus, A., and Tassinari, C., 2002, The Late-Variscan fault network in central-northern Portugal (NW Iberia): A re-evaluation: Tectonophysics, v. 359, no. 3–4, p. 255–270, doi:10.1016/S0040-1951(02)00514-0.

Marshak, S., 1988, Kinematics of orocline and arc formation in thin-skinned orogens: Tectonics, v. 7, no. 1, p. 73–86, doi:10.1029/TC007i001p00073.

Marshak, S., 2004, Salients, recesses, arcs, oroclines, and syntaxes—A review of ideas concerning the formation of map-view curves in fold-and-thrust belts, *in* McClay, K.R., ed., Thrust Tectonics and Hydrocarbon Systems: American Association of Petroleum Geologists Memoir 82, p. 131–156.

Marshak, S., and Wilkerson, M.S., 1992, Effect of overburden thickness on thrust belt geometry and development: Tectonics, v. 11, no. 3, p. 560–566, doi:10.1029/92TC00175.

Martínez, F.J., and Rolet, J., 1988, Late Paleozoic metamorphism in the northwestern Iberian Peninsula, Brittany, and related areas in SW Europe, *in* Harris, A.L., and Fettes, D.J., eds., The Caledonian-Appalachian Orogen: Geological Society of London Special Publication 38, p. 611–620.

Martínez-Catalán, J.R., 1990, A noncylindrical model for the northwest Iberian allochthonous terranes and their equivalents in the Hercynian belt of Western Europe: Tectonophysics, v. 179, p. 253–272, doi:10.1016/0040-1951(90)90293-H.

Martínez-Catalán, J.R., Arenas, R., García, F.D., and Abati, J., 1997, Variscan accretionary complex of northwest Iberia: Terrane correlation and succession of tectonothermal events: Geology, v. 25, p. 1103–1106, doi:10.1130/0091-7613(1997)025<1103:VACONI>2.3.CO;2.

Martínez-Catalán, J.R., Arenas, R., García, F.D., Cuadra, P.G., Gómez-Barreiro, J., Abati, J., Castiñeiras, P., Fernández-Suárez, J., Martínez, S.S., Andonaegui, P., Clavijo, E.G., Montes, A.D., Pascual, F.J.R., and Aguado, B.V., 2007, Space and time in the tectonic evolution of the northwestern Iberian Massif: Implications for the Variscan belt, *in* Hatcher, R.D., Jr., Carlson, M.P., McBride, J.H., and Martínez Catalán, J.R., eds., 4-D Framework of Continental Crust: Geological Society of America Memoir 200, p. 403–423, doi:10.1130/2007.1200(21).

Martínez-Catalán, J.R., Arenas, R., Abati, J., Sánchez-Martínez, S., Díaz-García, F., Fernández-Suárez, J., González Cuadra, P., Castiñeiras, P., Gómez-Barreiro, J., Díez Montes, A., González Clavijo, E., Rubio Pascual, F.J., Andonaegui, P., Jeffries, T.E., Alcock, J.E., Díez Fernández, R., and López-Carmona, A., 2009, A rootless suture and the loss of the roots of a mountain chain: The Variscan belt of NW Iberia: Comptes Rendus Geoscience, v. 341, no. 2–3, p. 114–126, doi:10.1016/j.crte.2008.11.004.

Martin-Izard, A., Fuertes-Fuente, M., Cepedal, A., Moreiras, D., Nieto, J.G., Maldonado, C., and Pevida, L.R., 2000, The Rio Narcea gold belt intrusions: Geology, petrology, geochemistry and timing: Journal of Geochemical Exploration, v. 71, no. 2, p. 103–117, doi:10.1016/S0375-6742(00)00148-5.

Matte, P., 2001, The Variscan collage and orogeny (480–290 Ma) and the tectonic definition of the Armorica microplate: A review: Terra Nova, v. 13, no. 2, p. 122–128, doi:10.1046/j.1365-3121.2001.00327.x.

Matte, P., and Ribeiro, A., 1975, Forme et orientation de l'ellipsoide de deformation dans la viration Hercynienne de Galicia: Relation avec le plissement et hypotheses sur la genese de l'arc Iberio-Armoricain: Comptes Rendus de l'Academie des Sciences, v. 280, p. 2825–2828.

McClay, K.R., 1976, The rheology of plasticine: Tectonophysics, v. 33, no. 1–2, p. T7–T15, doi:10.1016/0040-1951(76)90047-0.

McClay, K.R., and Ellis, P.G., 1987, Analogue models of extensional fault geometries, *in* Coward, M.P., Dewey, J.F., and Hancock, P.L., eds., Continental extensional tectonics: Geological Society of London Special Publication 28, p. 109–125.

Merino-Tomé, O.A., Bahamonde, J.R., Colmenero, J.R., Heredia, N., Villa, E., and Farias, P., 2009, Emplacement of the Cuera and Picos de Europa imbricate system at the core of the Iberian-Armorican Arc (Cantabrian zone, north Spain): New precisions concerning the timing of arc closure: Geological Society of America Bulletin, v. 121, no. 5–6, p. 729–751, doi:10.1130/B26366.1.

Mitra, G., 1997, Evolution of salients in a fold-and-thrust belt: The effects of sedimentary basin geometry, strain distribution and critical taper, *in* Sengupta, S., Ghosh, S.K., and Naha, K., eds., Evolution of Geological Structures from Macro- to Micro-Scales: London, Chapman and Hall, p. 59–90.

Morency, C., and Doin, M.-P., 2004, Numerical simulations of the mantle lithosphere delamination: Journal of Geophysical Research, v. 109, p. B03410, doi:10.1029/2003JB002414.

Morency, C., Doin, M.-P., and Dumoulin, C., 2002, Convective destabilization of a thickened continental lithosphere: Earth and Planetary Science Letters, v. 202, no. 2, p. 303–320, doi:10.1016/S0012-821X(02)00753-7.

Moresi, L., Dufour, F., and Mühlhaus, H.-B., 2002, Mantle convection modeling with viscoelastic/brittle lithosphere: Numerical methodology and plate tectonic modeling: Pure and Applied Geophysics, v. 159, no. 10, p. 2335–2356, doi:10.1007/s00024-002-8738-3.

Muñoz-Quijano, I.N., and Gutiérrez-Alonso, G., 2007a, Modelo de evolución topográfica en el NO de la Península Ibérica durante la delaminación litosférica al final de la Orogenia Varisca: Geogaceta, v. 43, p. 43–46.

Muñoz-Quijano, I.N., and Gutiérrez-Alonso, G., 2007b, Respuesta topográfica a un proceso de delaminación litosférica: Un modelo simple para el final del Orógeno Varisco en el NO de la Península Ibérica: Studia Geologica Salmanticensia, v. 43, no. 2, p. 175–192.

Narr, W., and Suppe, J., 1991, Joint spacing in sedimentary rocks: Journal of Structural Geology, v. 13, no. 9, p. 1037–1048, doi:10.1016/0191-8141(91)90055-N.

Nijman, W., and Savage, J., 1989, Persistent basement wrenching as controlling mechanism of Variscan thin-skinned thrusting and sedimentation, Cantabrian Mountains Spain: Tectonophysics, v. 169, no. 4, p. 281–302, doi:10.1016/0040-1951(89)90092-9.

Pastor-Galán, D., Gutiérrez-Alonso, G., and Weil, A.B., 2011, Orocline timing through joint analysis. Insights from the Ibero-Armorican Arc: Tectonophysics, v. 507, no. 1–4, p. 31–46, doi:10.1016/j.tecto.2011.05.005.

Pastor-Galán, D., Gutiérrez-Alonso, G., Mulchrone, K.F., and Huerta, P., 2012, Conical folding in the core of an orocline. A geometric analysis from the Cantabrian Arc (Variscan belt of NW Iberia): Journal of Structural Geology (in press).

Paulsen, T., and Marshak, S., 1999, Origin of the Uinta recess, Sevier fold-thrust belt, Utah: Influence of basin architecture on fold-thrust belt geometry: Tectonophysics, v. 312, no. 2–4, p. 203–216, doi:10.1016/S0040-1951(99)00182-1.

Pérez-Estaún, A., Bastida, F., Alonso, J.L., Marquinez, J., Aller, J., Álvarez-Marrón, J., Marcos, A., and Pulgar, J.A., 1988, A thin-skinned tectonics model for an arcuate fold and thrust belt—The Cantabrian zone (Variscan Ibero-Armorican Arc): Tectonics, v. 7, no. 3, p. 517–537, doi:10.1029/TC007i003p00517.

Pérez-Estaún, A., Bastida, F., Alonso, J.L., Marquinez, J., Aller, J., Álvarez-Marrón, J., Farias, P., Marcos, A., and Pulgar, J.A., 1991, The Cantabrian zone—An interpretation for an arcuate foreland thrust belt: Tectonophysics, v. 191, no. 3–4, p. 435, doi:10.1016/0040-1951(91)90090-F.

Pérez-Estaún, A., Pulgar, J.A., Banda, E., Álvarez-Marrón, J., Marcos, A., Bastida, F., Alonso, J.L., Aller, J., Farias, P., Martínez-Catalán, J.R., Comas, M.C., Danobeitia, J.J., and Cordoba, D., 1994, Crustal structure of the external Variscides in northwest Spain from deep seismic-reflection profiling: Tectonophysics, v. 232, no. 1–4, p. 91–118, doi:10.1016/0040-1951(94)90078-7.

Pysklywec, R.N., 2006, Surface erosion control on the evolution of the deep lithosphere: Geology, v. 34, no. 4, p. 225–228, doi:10.1130/G21963.1.

Pysklywec, R.N., and Cruden, A.R., 2004, Coupled crust-mantle dynamics and intraplate tectonics: Two-dimensional numerical and three-dimensional analogue modeling: Geochemistry, Geophysics, Geosystems, v. 5, Q10003, doi:10.1029/2004GC000748.

Pysklywec, R.N., Beaumont, C., and Fullsack, P., 2002, Lithospheric deformation during the early stages of continental collision: Numerical experiments and comparison with South Island, New Zealand: Journal of Geophysical Research, v. 107, p. 2133, doi:10.1029/2001JB000252.

Pysklywec, R.N., Gogus, O., Percival, J., Cruden, A.R., and Beaumont, C., 2010, Insights from geodynamical modeling on possible fates of continental mantle lithosphere: Collision, removal, and overturn: Canadian Journal of Earth Sciences, v. 47, no. 4, p. 541–563, doi:10.1139/E09-043.

Ribeiro, A., Dias, R., and Silva, J.B., 1995, Genesis of the Ibero-Armorican Arc: Geodinamica Acta, v. 8, no. 4, p. 173–184.

Ribeiro, A., Munha, J., Dias, R., Mateus, A., Pereira, E., Ribeiro, L., Fonseca, P., Araujo, A., Oliveira, T., Romao, J., Chamine, H., Coke, C., and Pedro, J., 2007, Geodynamic evolution of the SW Europe Variscides: Tectonics, v. 26, no. 6, TC6009, doi:10.1029/2006TC002058.

Ries, A.C., and Shackleton, R.M., 1976, Patterns of strain variation in arcuate fold belts: Philosophical Transactions of the Royal Society of London, ser. A, Mathematical and Physical Sciences, v. 283, no. 1312, p. 281–288, doi:10.1098/rsta.1976.0085.

Rossi, D., and Storti, F., 2003, New artificial granular materials for analogue laboratory experiments: Aluminium and siliceous microspheres: Journal of Structural Geology, v. 25, no. 11, p. 1893–1899, doi:10.1016/S0191-8141(03)00041-5.

Rydelek, P.A., and Sacks, I.S., 1988, Asthenospheric viscosity inferred from correlated land-sea earthquakes in north-east Japan: Nature, v. 336, no. 6196, p. 234–237, doi:10.1038/336234a0.

Schott, B., and Schmeling, H., 1998, Delamination and detachment of a lithospheric root: Tectonophysics, v. 296, no. 3–4, p. 225–247, doi:10.1016/S0040-1951(98)00154-1.

Schöpfer, M.P.J., and Zulauf, G.A., 2002, Strain-dependent rheology and the memory of plasticine: Tectonophysics, v. 354, no. 1-2, p. 85–99.

Shemenda, A.I., and Grocholsky, A.L., 1992, Physical modelling of lithosphere subduction in collision zones: Tectonophysics, v. 216, no. 3–4, p. 273–290, doi:10.1016/0040-1951(92)90401-Q.

Shi, Y., and Cao, J., 2008, Lithosphere effective viscosity of continental China: Earth Science Frontiers, v. 15, no. 3, p. 82–95, doi:10.1016/S1872-5791(08)60064-0.

Simancas, J., Azor, A., Martínez-Poyatos, D., Tahiri, A., El Hadi, H., González-Lodeiro, F., Pérez-Estaún, A., and Carbonell, R., 2009, Tectonic relationships of southwest Iberia with the allochthons of northwest Iberia and the Moroccan Variscides: Comptes Rendus Geoscience, v. 341, no. 2–3, p. 103–113, doi:10.1016/j.crte.2008.11.003.

Stampfli, G.M., and Borel, G.D., 2002, A plate tectonic model for the Paleozoic and Mesozoic constrained by dynamic plate boundaries and restored synthetic oceanic isochrons: Earth and Planetary Science Letters, v. 196, no. 1–2, p. 17–33, doi:10.1016/S0012-821X(01)00588-X.

Stewart, S.A., 1995, Paleomagnetic analysis of fold kinematics and implications for geological models of the Cantabrian/Asturian arc, north Spain: Journal of Geophysical Research–Solid Earth, v. 100, p. 20,079–20,094, doi:10.1029/95JB01482.

Suess, E., 1885, Das Antlitz der Erde: Vienna, Austria, F. Tempsky, 776 p.

Tapponnier, P., Peltzer, G., Le Dain, A.Y., Armijo, R., and Cobbold, P., 1982, Propagating extrusion tectonics in Asia: New insights from simple experiments with plasticine: Geology, v. 10, no. 12, p. 611–616, doi:10.1130/0091-7613(1982)10<611:PETIAN>2.0.CO;2.

Tkalcec, B., 2010, Variscan Orogenic Collapse in the Bohemian Massif: Results from Analogue Modelling [Ms.C. thesis]: Frankfurt am Main, Germany, Goethe Universität, 87 p.

Touloukian, Y.S., Powell, R.W., Ho, C.Y., and Klemens, P.C., 1970, Thermophysical Properties of Matter: Volume 2. Thermal Conductivity: Nonmetallic Solids: New York, Defense Technical Information Center, 1389 p.

Treloar, P.J., and Coward, M.P., 1991, Indian plate motion and shape: Constraints on the geometry of the Himalayan orogen: Tectonophysics, v. 191, no. 3–4, p. 189–198, doi:10.1016/0040-1951(91)90055-W.

Valverde-Vaquero, P., 1992, Permo-Carboniferous Magmatic Activity in the Cantabrian Zone (N.E. Iberian Massif, Asturias, NW Spain) [Ph.D. thesis]: Boston, Massachusetts, Boston College, 498 p.

Van der Voo, R., Stamatakos, J.A., and Pares, J.M., 1997, Kinematic constraints on thrust-belt curvature from syndeformational magnetizations in the Lagos del Valle syncline in the Cantabrian Arc, Spain: Journal of Geophysical Research–Solid Earth, v. 102, no. B5, p. 10,105–10,119, doi:10.1029/97JB00263.

Walcott, R.I., 1970, Isostatic response to loading of the crust in Canada: Canadian Journal of Earth Sciences, v. 7, no. 2, p. 716–727, doi:10.1139/e70-070.

Weijermars, R., 1986, Flow behaviour and physical chemistry of bouncing putties and related polymers in view of tectonic laboratory applications: Tectonophysics, v. 124, no. 3–4, p. 325–358, doi:10.1016/0040-1951(86)90208-8.

Weijermars, R., and Schmeling, H., 1986, Scaling of Newtonian and non-Newtonian fluid dynamics without inertia for quantitative modeling of rock flow due to gravity (including the concept of rheological similarity): Physics of the Earth and Planetary Interiors, v. 43, p. 316–330, doi:10.1016/0031-9201(86)90021-X.

Weil, A.B., 2006, Kinematics of orocline tightening in the core of an arc: Paleomagnetic analysis of the Ponga Unit, Cantabrian Arc, northern Spain: Tectonics, v. 25, no. 3, TC3012, doi:10.1029/2005TC001861.

Weil, A.B., and Sussman, A.J., 2004, Classifying curved orogens based on timing relationships between structural development and vertical-axis rotations, *in* Sussman, A.J., and Weil, A.B., eds., Orogenic Curvature: Integrating Paleomagnetic and Structural Analysis: Geological Society of America Special Paper 383, p. 1–16.

Weil, A.B., and Van der Voo, R., 2002, The evolution of the paleomagnetic fold test as applied to complex geologic situations, illustrated by a case study from northern Spain: Physics and Chemistry of the Earth, v. 27, no. 25–31, p. 1223–1235.

Weil, A.B., and Yonkee, A., 2009, Anisotropy of magnetic susceptibility in weakly deformed red beds from the Wyoming salient, Sevier thrust belt: Relations to layer-parallel shortening and orogenic curvature: Lithosphere, v. 1, no. 4, p. 235–256, doi:10.1130/L42.1.

Weil, A.B., Van der Voo, R., van der Pluijm, B.A., and Pares, J.M., 2000, The formation of an orocline by multiphase deformation: A paleomagnetic investigation of the Cantabria-Asturias Arc (northern Spain): Journal of Structural Geology, v. 22, no. 6, p. 735–756, doi:10.1016/S0191-8141(99)00188-1.

Weil, A.B., van der Voo, R., and van der Pluijm, B.A., 2001, Oroclinal bending and evidence against the Pangea megashear: The Cantabria-Asturias arc (northern Spain): Geology, v. 29, no. 11, p. 991–994, doi:10.1130/0091-7613(2001)029<0991:OBAEAT>2.0.CO;2.

Weil, A.B., Gutiérrez-Alonso, G., and Conan, J., 2010, New time constraints on lithospheric-scale oroclinal bending of the Ibero-Armorican Arc: A paleomagnetic study of earliest Permian rocks from Iberia: Journal of the Geological Society of London, v. 167, p. 127, doi:10.1144/0016-76492009-002.

Willingshofer, E., and Sokoutis, D., 2009, Decoupling along plate boundaries: Key variable controlling the mode of deformation and the geometry of collisional mountain belts: Geology, v. 37, no. 1, p. 39–42, doi:10.1130/G25321A.1.

Yonkee, A., and Weil, A.B., 2010, Reconstructing the kinematic evolution of curved mountain belts: Internal strain patterns in the Wyoming salient, Sevier thrust belt, U.S.A.: Geological Society of America Bulletin, v. 122, no. 1–2, p. 24–49, doi:10.1130/B26484.1.

Zeitler, P.K., Koons, P.O., Bishop, M.P., Chamberlain, C.P., Craw, D., Edwards, M.A., Hamidullah, S., Jan, M.Q., Khan, M.A., Khattak, M.U.K., Kidd, W.S.F., Mackie, R.L., Meltzer, A.S., Park, S.K., Pecher, A., et al., 2001, Crustal reworking at Nanga Parbat, Pakistan: Metamorphic consequences of thermal-mechanical coupling facilitated by erosion: Tectonics, v. 20, no. 5, p. 712–728, doi:10.1029/2000TC001243.

Zulauf, G., Zulauf, J., Hastreiter, P., and Tomandl, B., 2003, A deformation apparatus for three-dimensional coaxial deformation and its application to rheologically stratified analogue material: Journal of Structural Geology, v. 25, no. 3, p. 469–480, doi:10.1016/S0191-8141(02)00023-8.

Zulauf, J., and Zulauf, G., 2004, Rheology of plasticine used as rock analogue: The impact of temperature, composition and strain: Journal of Structural Geology, v. 26, no. 4, p. 725–737, doi:10.1016/j.jsg.2003.07.005.

Zulauf, J., and Zulauf, G., 2005, Coeval folding and boudinage in four dimensions: Journal of Structural Geology, v. 27, no. 6, p. 1061–1068, doi:10.1016/j.jsg.2005.04.003.

Zulauf, J., Zulauf, G., Kraus, R., and Gutiérrez-Alonso, G., 2011a, The origin of tablet boudinage: Results from experiments using power-law rock analogs: Tectonophysics, v. 510, p. 327–336, doi:10.1016/j.tecto.2011.07.013.

Zulauf, J., Zulauf, G., Hammer, J., and Zanella, F., 2011b, Tablet boudinage of an anhydrite layer in rock-salt matrix: Results from thermomechanical experiments: Journal of Structural Geology, v. 33, p. 1801–1815, doi:10.1016/j.jsg.2011.09.006.

Science Editor: Christian Koeberl
Associate Editor: Andrew Hynes

Manuscript Received 7 November 2011
Revised Manuscript Received 27 January 2012
Manuscript Accepted 30 January 2012

Printed in the USA